Chapter 7

Numerical Computation of Riser Dynamics

C. P. Pesce & C. A. Martins
Escola Politécnica, University of São Paulo

7.1 Introduction

Risers are pipes that connect the floating production structure to the sea floor. Their primary function is to transport the oil produced at the "Christmas Tree" installed on the wellhead at the seabed to the floating unit. Additionally, there is a need to control subsea valves, inject gas or water into the reservoir and transfer oil or gas from one floating system to another. At the same time, exploitation of hydrocarbons in deeper waters made the use of floating systems more common. Such a trend has strongly motivated recent research activities on risers, mainly related to the dynamic problem. There are several types of risers, designed to meet the specifications of a particular application. A worldwide trend in the offshore oil industry is to use, whenever possible, a simple and cost-effective system: the catenary riser.

A *catenary riser* is a free-hanging riser with no intermediate buoys or floating devices. This kind of system is subject to dynamic loads caused by the action of current, waves and excited by the FPU (floating production unit) motions, imposed at the top extremity (hang-off). Figure 7.1 shows a view of typical systems.

Current induces static and dynamic loads, including those related to vortex shedding. The direct action of sea waves causes oscillatory loads, in a wide range of frequencies, but restricted to a region near the surface. However, motions imposed by the FPU at the top connection of the riser cause the most significant loads. The vessel oscillates in two different frequency ranges. The first one is the same range that characterizes the surface waves. The second one is associated to the well-known slow-drift motions. These two actions make the riser move, displacing dynamically the touchdown point (TDP) on the seabed.

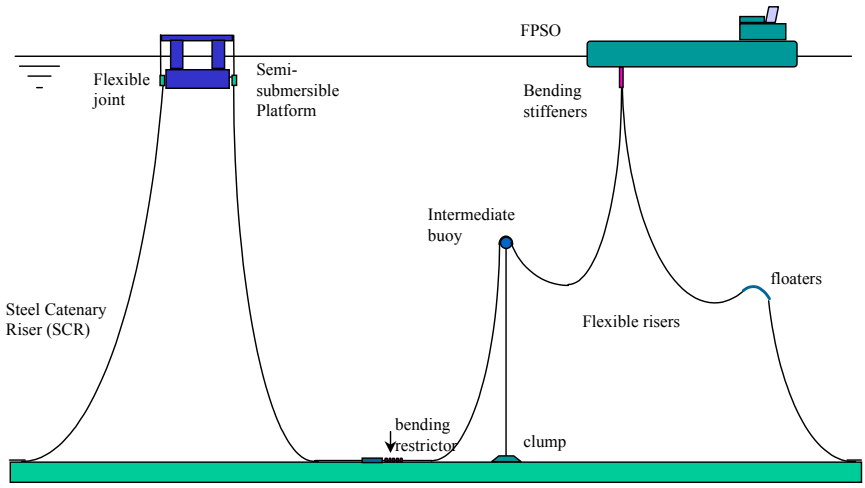

Figure 7.1: Floating production systems and risers. Mooring lines are not shown.

There are at least three different time-scales in the catenary riser problem; see, e.g. Triantafyllou et al. (1985). The first one is dominated by axial rigidity, giving rise to relatively small periods of oscillation. The second one is related to the catenary or geometric rigidity. The third one is of a local nature and is due to the local flexural rigidity effects. Such a diversity of time-scales can lead to serious limitations concerning numerical integration methods by rendering dynamic equations mathematically stiff.

Even the starting problem, to determine the static configuration, can pose serious numerical difficulties, as the flexural rigidity effect is confined and dominant just inside small regions close to the ends, the TDP (touch-down point) and the upper end-fitting or close to other regions of high curvatures. The boundary condition at TDP is of the contact type, geometrically nonlinear. Other highly nonlinear phenomena in cables have also been addressed in recent years by a number of authors, as in Newberry and Perkins (1997); Leissa and Saad (1994). Numerous numerical methods have been discussed and implemented in the last two decades; see, e.g., Leira and Remseth (1985), Larsen (1992). An extensive review on modeling and analysis methods can be found in Patel and Seyed (1995), who pointed out a number of research points that should deserve special consideration. One of them is related to the riser-soil contact modeling. Almost a decade has passed and this particular issue has not been addressed comprehensively.

Regarding the global dynamic problem, most of the efforts have been directed to nonlinear numerical schemes. The above-mentioned multiplicity of time-scales enforces the development and use of highly robust numerical methods. Even though, full nonlinear numerical simulations in the time domain are really time consuming. Therefore, more appropriate for analysis, rather than for design tasks, when hundreds of cases and environmental conditions have to be accounted for. Actually, time-domain simulations are worthwhile in a number of situations. Most of them are related to (see, e.g., API-2RD Recommended

Practice (1998)): large displacements, tension coupling, nonlinear loading, foundation modeling. Others that should be cited are those related to transient events, such as pull-in/pull-out/disconnecting operations, loss of FPU station-keeping ability, mooring-system failures, etc. Time-domain simulations are also worthwhile in providing a reference for equivalent frequency-domain analysis, the latter used in extensive design work, or as a checking tool for the response in severe environmental conditions, where nonlinear behaviour would prevail.

On the other hand, the above-mentioned particularities may enable asymptotic approaches to be rather effective. As an example, the local nature of the flexural-rigidity effect allows the global dynamic problem, under the ideal cable equation in the frequency-domain, to be treated by standard perturbation techniques, with tremendous gains in processing time. The local non-linear effects, due to the geometric non-linear boundary conditions in the TDP region, can be included by means of a standard boundary-layer technique; Aranha et al. (1997)[1], Pesce et al. (1998a). The boundary-layer technique can also be applied for the local solution in the upper connection region, or else to incorporate the effect of soil elasticity in the TDP region. Another kind of asymptotic solution can be constructed, for the dynamic tension response, making use of the disparity between the first and the second time-scales. In this latter analytical solution the dynamic tension response to oscillatory excitation applied at the top, in the presence of waves and current, has been determined and experimentally/numerically confirmed for a full range of exciting frequencies; Aranha et al. (1993), Aranha and Pinto (2001).

An important issue that also deserves special attention is the dynamic compression of risers under curvature. Numerical solutions compare well with planar analytical solutions (Aranha et al. (2001a), but still expect to be verified with analytical solutions that include twist; Ramos and Pesce (2003).

Another essential subject is the eigenvalue problem for catenary risers, particularly pertinent for vortex-induced vibration (VIV) analysis. An analytical and closed-form WKB approximate solution, previously derived by Triantafyllou (1984), may be applied to the catenary-riser problem, given the tension function along the length; see also Pesce et al. (1999). Numerical results obtained with codes based on the Finite Element Method (FEM) compare well with the asymptotic solution. However, VIV in risers, particularly in catenary risers, is still an open research subject. Many fundamental issues in this important phenomenon remain to be understood and modeled; Sarpkaya (2003). Some open issues of substantial importance for riser dynamics may be cited, as for example, multi-modal simultaneous excitation, curvature effects, influence and coupling of VIV with the dynamics in other time-scales, sub-harmonic resonance that couples stream and cross-wise displacements, etc. Much of the VIV phenomenon is already covered in this book and therefore will not be treated in the present chapter.

This chapter aims to address the dynamics of risers. Even though the numerical approach is the ultimate goal, analytical approaches serve as a basis for insight and discussion. For didactic purposes we restrain ourselves to treat the

[1] Similar problems, concerning stresses in cables, have been treated with the same approach; see, e.g. Irvine (1992).

simple and basic planar case of a free-hanging riser, not entering deeply into the discussion on hydrodynamic loads, particularly on VIV.

7.2 The Static Planar Problem

Consider the planar problem in the arch-length coordinate s. From the general Kirchoff-Clebsh-Love equations, the static equilibrium can be written

$$\begin{aligned} &\frac{dT}{ds} - Q\frac{d\theta}{ds} + f_t = 0 \\ &\frac{dQ}{ds} + T\frac{d\theta}{ds} + f_n = 0 \\ &EI\frac{d^2\theta}{ds^2} + Q = 0 \ . \end{aligned} \tag{7.1}$$

$T(s)$ is the effective tension, $Q(s)$ the shear force, EI is the 'equivalent' bending stiffness, $\theta(s)$ the angle with respect to the horizontal line and

$$\begin{aligned} f_n &= -q\cos\theta + c_n(s) \\ f_t &= -qsen\theta + c_t(s) \end{aligned} \tag{7.2}$$

are the normal and tangential components of forces per unit length, with q the immersed weight and $c_n(s)$ and $c_t(s)$ the corresponding steady hydrodynamic forces due to the current action.

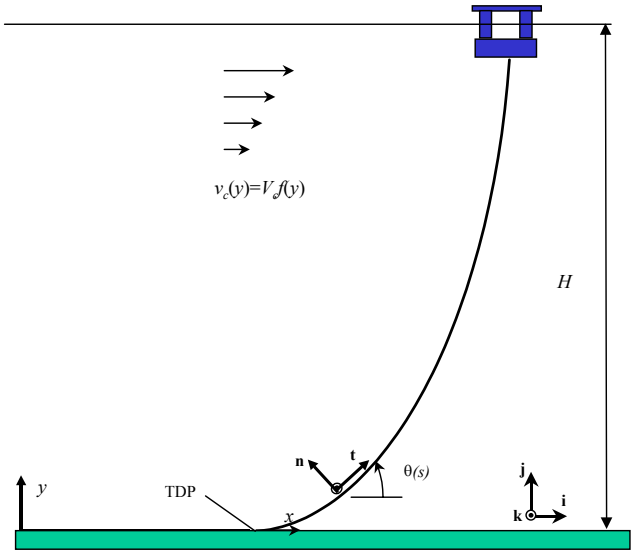

Figure 7.2: The static planar problem.

It is possible to eliminate $T(s)$ and $Q(s)$, resulting in a non-linear integral-differential equation in $\theta(s)$; see Love, art. 273[A],[2]

$$EI\frac{d^2\theta}{ds^2}\sec\theta + qs - \int_0^s \left(c_n \sec\theta + \sec^2\theta \left(\frac{d\theta}{ds}\right) \int_0^\xi \left(c_n sen\theta - c_t \cos\theta\right) d\xi \right) ds = \\ = T_0 \tan\theta - Q_0 \ , \tag{7.3}$$

where $T_0 = T(0)$ and $Q_0 = Q(0)$, at TDP. Equation (7.3) shows explicitly that, as current forces are functions of $\theta(s)$, the solution must be found iteratively.

In the absence of current action, in non-dimensional form

$$\varepsilon^2 \frac{d^2\theta}{d\hat{s}^2}\sec\theta + \hat{q}\hat{s} = \tan\theta + \hat{Q}_0 \\ \lambda^2 = EI/T_0 \ ; \ \ \varepsilon = \lambda/L \ ; \ \ \hat{s} = s/L \ ; \ \ \hat{q} = qL/T_0 \ ; \ \ \hat{Q}_0 = Q_0/T_0 \tag{7.4}$$

L being the suspended length and λ the flexural length scale at TDP. The small nondimensional number $\varepsilon = \lambda/L$ gauges the small importance of flexural rigidity, in the global static problem, if compared to the geometric rigidity. Equation (7.4) is a singular perturbation problem and the reason for many numerical difficulties; see, e.g., Kevorkian and Cole (1981). Note that if bending effects are neglected, the classical catenary equation is obtained (c is used for the ideal catenary),

$$\tan\theta_c(s_c) = \chi_{0c} s_c \tag{7.5}$$

with $\chi_{0c} = q/T_{0c}$ the ideal catenary static curvature at TDP. The corresponding curvature and effective tension functions are

$$\chi_c(s_c) = \frac{d\theta_c}{ds_c} = \chi_{0c}\cos^2\theta_c(s_c) = \chi_{0c}\frac{1}{1+(\chi_{0c}s_c)^2} \ , \tag{7.6}$$

$$T_c(s_c) = T_{0c}\sec\theta_c \ . \tag{7.7}$$

7.2.1 The ideal string equations

If Cartesian coordinates are used instead and neglecting flexural-rigidity effects, the equilibrium equations can be written,

$$\frac{dx}{ds} = (1+\varepsilon)\cos\theta \ ; \qquad \frac{dz}{ds} = (1+\varepsilon)\sin\theta$$

$$\frac{dF_x}{ds} = -c_x \ ; \qquad \frac{dF_z}{ds} = q - c_z \tag{7.8}$$

$$\frac{d\theta}{ds} = \frac{f_n}{T} \ ; \qquad \varepsilon = \frac{N}{EA} \ ,$$

[2] See Bernitsas and Korakakis (1988), for an analysis of the importance of non-linearities.

where $T = F_x \cos\theta + F_y sen\theta$, N is the traction and EA the equivalent axial rigidity. In eqn (7.8),

$$c_x = \frac{1}{2} c_d \, D \, \rho_a V_c^2 f(y) sen^2\theta \mid f(y) sen\theta \mid$$
$$c_y = -\frac{1}{2} c_d \, D \, \rho_a V_c^2 f(y) sen\theta \cos\theta \mid f(y) sen\theta \mid \quad (7.9)$$

are components of the current drag force, considering only the drag coefficient normal to the line (tangential friction is here neglected). $v_c(y) = V_c f(y(s))$ is the local current profile.

If the string is considered non-extensible the equilibrium equations take the simplest form,

$$\frac{dx}{ds} = \cos\theta \; ; \qquad \frac{dz}{ds} = sen\theta$$
$$\frac{dF_x}{ds} = -c_x \; ; \qquad \frac{dF_z}{ds} = q - c_z \quad (7.10)$$
$$\frac{d\theta}{ds} = \frac{f_n}{T} \; ;$$

where $x(s)$, $y(s)$, $F_x(s)$, $F_y(s)$ e $\theta(s)$ are the unknowns. An additional unknown is the curvilinear TDP coordinate s_0 (or instead the suspended length L). Hence, ℓ_t being the total length, assuming for simplicity the soil as horizontal and taking for convenience $s_0 = 0$, the corresponding boundary conditions are

$$x(0) = 0 \; ; \; y(0) = 0 \; ; \; \theta(0) = 0 \; ; \; F_z(0) = 0 \; ; \; x(L) = x_t - (\ell_t - L) \; ; \; y(L) = y_t \; . \quad (7.11)$$

As L is an unknown, the solution procedure is iterative.

7.2.2 Numerical solution

As $F_x(0)$ is the only unknown at the origin, an iterative algorithm where $F_x(0)$ is varied at each integration step is recommended to solve the equilibrium equations (7.8).

7.2.2.1 Iteration procedure

Apart from the hang-off section, the following inequality is valid

$$s - x(s) < \ell_t - x(L) \; . \quad (7.12)$$

And, at the hang-off

$$s - x(s) = \ell_t - x(L) \; . \quad (7.13)$$

The following general algorithm can be easily implemented.

1. From the ideal catenary equation we take an initial shooting value for $F_x(0)$.
2. Equation (7.8) is integrated with respect to s and, at each step, the constraint (7.12) is verified.

3. Let s^* be the coordinate from which eqn (7.12) is no longer satisfied. If $|y(s^*) - y_t| \le \delta$ the problem is solved. Otherwise, (a) if $y(s^*) < y(L)$, this means that the assumed value $F_x(0)$ is not large enough (the line is slack) and we take $F_x{}^{k+1}(0) = F_x{}^{k}(0) + \delta F_x$, returning to step (2); (b) if $y(s^*) > y(L)$, the assumed value $F_x(0)$ is larger than required (the line is tight) and we take $F_x{}^{k+1}(0) = F_x{}^{k}(0) - \delta F_x$, returning to step (2).

7.2.2.2 Runge-Kutta auto-adaptive step method

To solve the equilibrium equations an iterative and explicit numerical scheme is recommended. A good choice is the classical, auto-adaptive step, Runge-Kutta method. Step sizing must be based on regions of larger curvature - in the present free-hanging case, on the TDP region.

7.2.3 The flexural-rigidity effect at extremities via boundary-layer technique

The equilibrium solution obtained for the extensible string equations can be corrected by applying a standard boundary-layer-technique approach (see, e.g., Bender & Orszag (1978)) in the regions of high curvature: TDP and top. We shall treat the hang-off region in section 7.3.6, under a dynamic approach.

7.2.3.1 TDP boundary layer. The rigid-soil case

Let $s = s_f$ be the actual TDP, when the flexural rigidity effect is taken into account. It can be easily shown that the hydrodynamic force term in eqn (7.3) is locally of order θ^2; $\theta << 1$. We can thus write, with an error of order θ^2,

$$\frac{d^2\chi}{ds^2} - \frac{1}{\lambda^2}\chi = -\frac{1}{\lambda^2}\chi_0; \quad s > s_f \ , \tag{7.14}$$

where $Q_0 = EI\left.\frac{d^3\theta}{ds^3}\right|^{s=s_f{}^+}$ is the shear force at $s = s_f{}^+$, for which $\theta = 0$.

Assuming a rigid flat bottom and null curvature at the actual TDP, i.e., enforcing continuity for the curvature at $s = s_f$, such that $\chi(s_f{}^+) = 0$ and $\chi(s) \equiv 0; \quad s \le s_f$, eqn (7.14) can be easily integrated giving rise to a local solution of the form,

$$\chi(s) = \begin{cases} \chi_0\left(1 - e^{-(1+s/\lambda)}\right); & \text{if} \quad s \ge -\lambda \\ 0 & \text{if} \quad s < -\lambda \end{cases} \tag{7.15}$$

$$\theta(s) = \begin{cases} \chi_0\lambda\left(\frac{s}{\lambda} + e^{-(1+s/\lambda)}\right); & \text{if} \quad s \ge -\lambda \\ 0 & \text{if} \quad s < -\lambda \end{cases} . \tag{7.16}$$

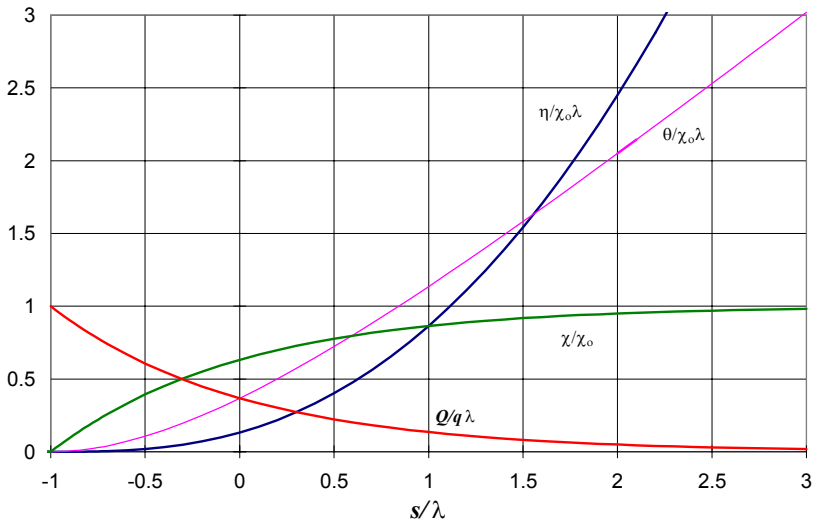

Figure 7.3: Local static solution in the TDP boundary layer. Rigid soil case. Nondimensional normalized curves for: $\eta/(\chi_0\lambda)$, $\theta/(\chi_0\lambda)$, χ/χ_0 and $|Q|/(q\lambda)$, respectively, local *elastica*, angle with respect to the horizontal, curvature and shear force.

As $\theta(s_f)=0$, $s_f=-\lambda$. In words, the flexural rigidity effect displaces the actual TDP to the left with respect to the ideal cable TDP, by an amount λ. From eqn (7.4) we see that the shear force at the actual TDP, such that $s\to s_f{}^{+}=-\lambda$ is given by, $Q_0=-q\lambda$. This latter equation provides some new insight into the physical meaning for the λ parameter*:* it gives a measure for the order of magnitude of the length within which the Euler-beam solution matches the cable solution, the shear force decaying exponentially to zero. Moreover, λ gives a measure to properly define the mesh refinement at the TDP region.

Note that the rigid-soil assumption and the condition $\chi(s)\equiv 0;\ \ s\le s_f$ implies a discontinuity in the shear force, at the actual TDP, that takes the form ($H(\cdot)$ is the unitary step, Heaviside function),

$$\frac{Q}{q\lambda}=H\big((s-s_f)/\lambda\big)e^{-(1+s/\lambda)} \quad . \qquad (7.17),$$

Figure 7.3 shows the local nondimensional solution - in a rather general form. The nondimensional vertical coordinate describing the elastic line, $\eta=y/\lambda$, is normalized with respect to $\chi_0\lambda=(q/T_0)\lambda$. Note that the typical matching distance is of order 4λ .

7.2.3.2 The linear elastic-soil case

Continuity on shear can be enforced in the case of a deformable soil; Pesce et al. (1998b). We shall consider the case of a linear elastic soil, with k_s the corresponding rigidity per unit of length and penetration. As an expected result, the TDP is displaced forward in such a way that the curvature changes sign, asymptotically decaying to zero as $s/\lambda \to -\infty$, in an oscillatory way. Let $y(s)$ be the local solution for the *elastica*, and $y_r = -q/k$ be the static offset (penetration into the soil) far away from the TDP. For simplicity we also consider a non-detachment condition from the soil, for $s \le s_f$. The coordinate s_f defines the TDP, here taken as the point where the *elastica* touches the bottom, i.e., $y(s_f) = 0$. If the soil is not too soft, we can locally take, $\theta \cong dy/dx$ and with a second-order error in θ, $s \cong x$ and $\chi(s) \cong \chi(x) \cong d^2y/dx^2$. The non-dimensional equilibrium equation, with $\xi = x/\lambda$; $\eta = y/\lambda$, is then given by (η^I indicates the first derivative with respect to the local coordinate ξ),

$$\eta^{IV} - \eta^{II} + K\eta = -\frac{q\lambda}{T_0} = -\chi_0\lambda = \frac{Q_0}{T_0}, \tag{7.18}$$

where the nondimensional soil-rigidity parameter may be defined as

$$K = \frac{k_s\lambda^2}{T_0} = \frac{k_s\lambda^4}{EI} = \frac{k_s EI}{T_0^{\,2}} = \chi_0\lambda\frac{k_s\lambda}{q}. \tag{7.19}$$

Equation (7.18) has a homogeneous solution, $\eta(\xi) = \sum_{j=1}^{4} A_j e^{\varpi_j(\xi-\xi_f)}$; $\xi \le \xi_f$, with eigenvalues $\varpi_j = \pm\left(\sqrt{\left(1 \pm (1-4K)^{1/2}\right)/2}\right)$. For usual applications, however, $K >> 1$, so that eqn (7.18) can be written, with an error of order $\chi_0\lambda << 1$, $\eta^{IV} + K\eta \cong 0$. Taking $\eta(\xi_f) = 0$; $\lim_{\xi\to-\infty}\eta(\xi) = 0$ and matching the solution on the soil with the exponential boundary-layer solution – this latter is valid on the suspended part – we finally obtain:

$$\eta(\xi) = \frac{y(s)}{\lambda} = \chi_0\lambda\frac{\sqrt{2}}{K^{1/2}}\frac{1}{\sqrt{2}+K^{1/4}}\exp\left(\frac{K^{1/4}}{\sqrt{2}}(\xi-\xi_f)\right)\sin\left(\frac{K^{1/4}}{\sqrt{2}}(\xi-\xi_f)\right);\ \text{if } \xi \le \xi_f$$

or

$$\eta(\xi) = \frac{y(s)}{\lambda} = \chi_0\lambda\left(\frac{\xi^2-\xi_a^{\,2}}{2} - \frac{K^{1/4}}{\sqrt{2}+K^{1/4}}\left(e^{-(\xi-\xi_f)}-1\right)\right);\ \text{if } \xi > \xi_f \tag{7.20}$$

where

$$\xi_f = \frac{s_f}{\lambda} = \frac{1}{\sqrt{2}+K^{1/4}}\left(\frac{1}{K^{1/4}} - K^{1/4}\right) \tag{7.21}$$

is the TDP position, with respect to TDP of an ideal cable supported on rigid soil. Also,

$$\theta(\xi) \cong \eta^{I}(\xi) = \chi_0 \lambda \frac{1}{K^{1/4}} \frac{1}{\sqrt{2}+K^{1/4}} \exp\left(\frac{K^{1/4}}{\sqrt{2}}(\xi-\xi_f)\right) \times$$
$$\left\{\sin\left(\frac{K^{1/4}}{\sqrt{2}}(\xi-\xi_f)\right)+\cos\left(\frac{K^{1/4}}{\sqrt{2}}(\xi-\xi_f)\right)\right\}; \quad \text{if } \xi \le \xi_f \tag{7.22}$$

or

$$\theta(\xi) \cong \eta^{I}(\xi) = \chi_0 \lambda \left(\xi + \frac{K^{1/4}}{\sqrt{2}+K^{1/4}} e^{-(\xi-\xi_f)}\right); \quad \text{if } \xi > \xi_f$$

is the angle, with respect to horizontal. The curvature is given by,

$$\chi(\xi) \cong \frac{1}{\lambda}\eta^{II}(\xi) =$$
$$= \chi_0 \frac{\sqrt{2}}{\sqrt{2}+K^{1/4}} \exp\left(\frac{K^{1/4}}{\sqrt{2}}(\xi-\xi_f)\right) \times \cos\left(\frac{K^{1/4}}{\sqrt{2}}(\xi-\xi_f)\right); \quad \text{if } \xi \le \xi_f \tag{7.23}$$

or

$$\chi(\xi) \cong \frac{1}{\lambda}\eta^{II}(\xi) = \chi_0 \left(1 - \frac{K^{1/4}}{\sqrt{2}+K^{1/4}} e^{-(\xi-\xi_f)}\right); \quad \text{if } \xi > \xi_f$$

and the shear force by,

$$\frac{Q}{q\lambda} = \frac{\eta^{III}(\xi)}{\chi_0 \lambda} = \frac{K^{1/4}}{\sqrt{2}+K^{1/4}} \exp\left(\frac{K^{1/4}}{\sqrt{2}}(\xi-\xi_f)\right) \times$$
$$\left\{\cos\left(\frac{K^{1/4}}{\sqrt{2}}(\xi-\xi_f)\right)-\sin\left(\frac{K^{1/4}}{\sqrt{2}}(\xi-\xi_f)\right)\right\}; \quad \text{if } \xi \le \xi_f \,. \tag{7.24}$$

or

$$\frac{Q}{q\lambda} = \frac{\eta^{III}(\xi}{\chi_0 \lambda}) = \frac{K^{1/4}}{\sqrt{2}+K^{1/4}} \exp\left(-(\xi-\xi_f)\right); \quad \text{if } \xi > \xi_f$$

Figure 7.4 presents the actual TDP position, with respect to the TDP of an ideal cable supported on linear elastic soil, as a function of the soil-rigidity parameter $K >> 1$. Note that $\xi_f \to -1$ as $K \to \infty$, recovering the rigid-soil case.

Figure 7.5 refers to the boundary-layer solution for four different values of $K = 10;10^2;10^3;10^4$, compared to the rigid-soil case. Note that only in the rigid-soil case does the TDP position coincide with the horizontal tangency point. The transition in the static curvature is clearly smooth, as a result of soil elasticity.

The maximum asymptotically attained value, inside the suspended boundary layer, remains the same. Negative values are now present along the supported part, as expected. The soil elasticity removes the discontinuity in the shear force that occurs in the rigid soil case. As K is inversely proportional to $T_0^{\,2}$, there is an enormous variability according to the tensioning condition.

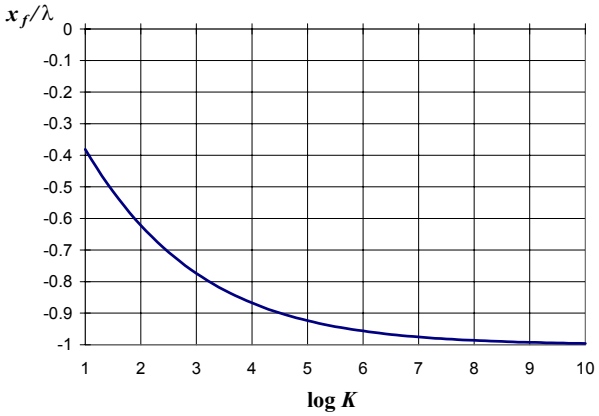

Figure 7.4: TDP position x_f/λ , with respect to the TDP of an ideal cable supported on rigid soil, as a function of the nondimensional soil rigidity parameter $K = k_s EI/T_0^2$.

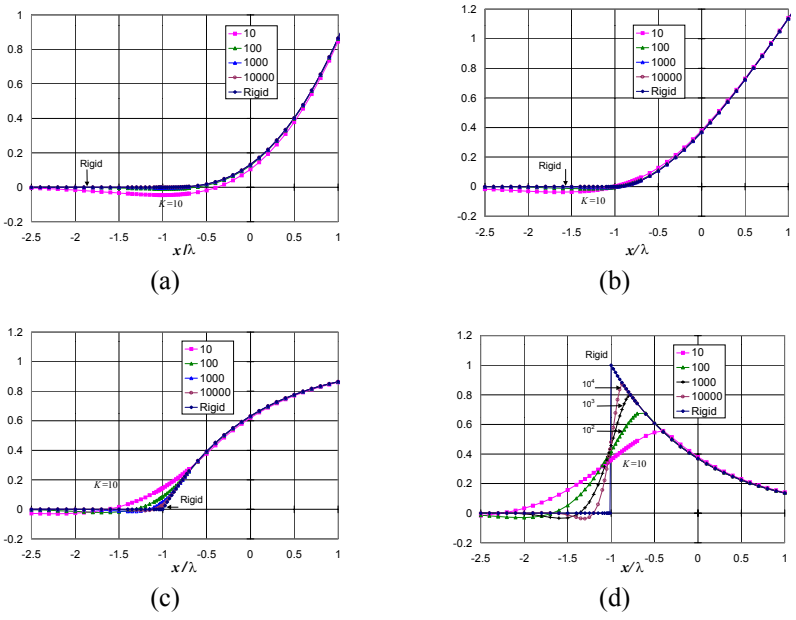

Figure 7.5: Local asymptotic solution for nondimensional: (a) elastica $\eta(\xi)/(\chi_0\lambda) = y(x)/(\chi_0\lambda^2)$; (b) angle with respect to the horizontal, $\theta(\xi)/\chi_0\lambda$; (c) nondimensional curvature, $\chi(\xi)/\chi_0$; (d) shear force, $Q(\xi)/q\lambda$; soil rigidity parameter $K = k_s EI/T_0^2$.

In typical steel catenary-riser cases we obtain $K > 10$. If umbilicals or flexible risers are considered instead, the nondimensional rigidity parameter K can take values of order 1 or even lower. In such cases, the complete solution of

eqn (7.18), under boundary conditions $\eta(0) = 0;\ \lim_{\xi \to -\infty} \eta(\xi) = -\chi_0 \lambda / K$, should be taken.

7.2.4 An illustrative example

As a case study we take a typical steel catenary riser to be installed in a semisubmersible platform in 1800 meters water depth. Table 7.1 presents the corresponding relevant data. Two cases are considered: (i) no current; (ii) current at surface, $V_c = +2m/s$, with a sheared triangular flow profile, such that $v_c(y) = V_c f(y);\ f(y) = 3y/2H - 1/3$. A Coulomb friction model has been used with friction coefficient $\mu = 0.4$ between the soil and the riser. The soil is supposed to be rigid. The string solution is corrected via the boundary-layer technique, so that the flexural-rigidity effect is taken into account in the TDP region. The riser is considered simply hinged at the top.

Table 7.1: SCR data.

Parameter		
Axial Rigidity EA (kN)	2.314 E+06	
Bending Stiffness EI (kNm^2)	9915	
Immersed weight q (kN/m)	0.727	
m (kg/m) (filled with water)	108.0	
External diameter D (m)	0.2032	
Thickness (mm)	19.05	
Depth H (m)	1800	
Total length (m)	5047	
Angle at top $\theta_L(^o)$ (no current)	70 (w.r.t. horizontal)	
	No current	With Current
Suspended length L (m)	2571	2447
Tension at TDP T_0 (kN)	680.55	719.23
Flexural length λ(m)	3.82	3.71
Curvature at TDP χ_0 (m^{-1})	1.077E-03	1.019E-03

Figure 7.6 shows examples of the elastic curve, effective tension and curvature ((a), (b) and (c)). Note the linear increase of tension on the soil due to Coulomb friction and that the TDP is slightly displaced to the left in the presence of current. Note also the abrupt increasing of curvature at TDP. Figure 7.3(d) zooms out of the TDP area, showing the effect of flexural rigidity, compared to the pure string case.

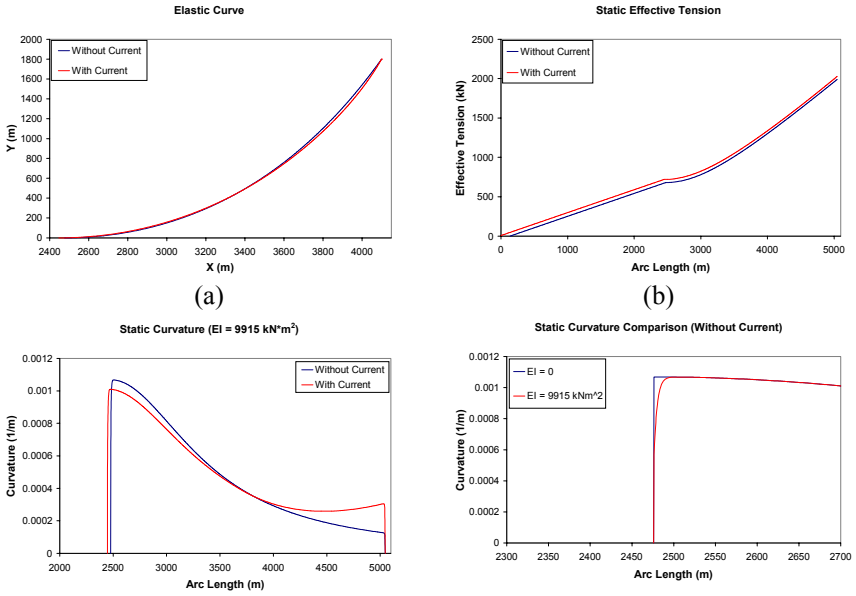

Figure 7.6: Static solution for a SCR. (a) Elastica; (b) Effective Tension (kN); (c) Curvature (1/m); (d) Local curvature at TDP (with and without flexural rigidity).

7.3 The Dynamic Planar Problem

The static configuration is given by the functions, $\theta(s)$ and $T(s)$. Let $u_t(s,t)$ and $u_n(s,t)$, *tangential* and *normal* displacements at s, be perturbations around the static equilibrium. Let also $\gamma(s,t), \tau(s,t), \vartheta(s,t), e(s,t)$ be, respectively, small perturbations of the variables: angle (w. r. t. horizontal), effective tension, shear force and axial deformation. Therefore, the total (static plus dynamic parcels) corresponding functions are given by,

$$\begin{aligned} \Theta(s,t) &= \theta(s) + \gamma(s,t) \\ T(s,t) &= T(s) + \tau(s,t) \\ Q(s,t) &= Q(s) + \vartheta(s,t) \\ \varepsilon(s,t) &= \varepsilon(s) + e(s,t) \ . \end{aligned} \tag{7.25}$$

Simple kinematic relations hold,

$$\begin{aligned} \frac{\partial u_n}{\partial s} + u_t \frac{d\theta}{ds} &= (1+\varepsilon(s))\gamma(s,t) \\ \frac{\partial u_t}{\partial s} - u_n \frac{d\theta_e}{ds} &= e \ . \end{aligned} \tag{7.26}$$

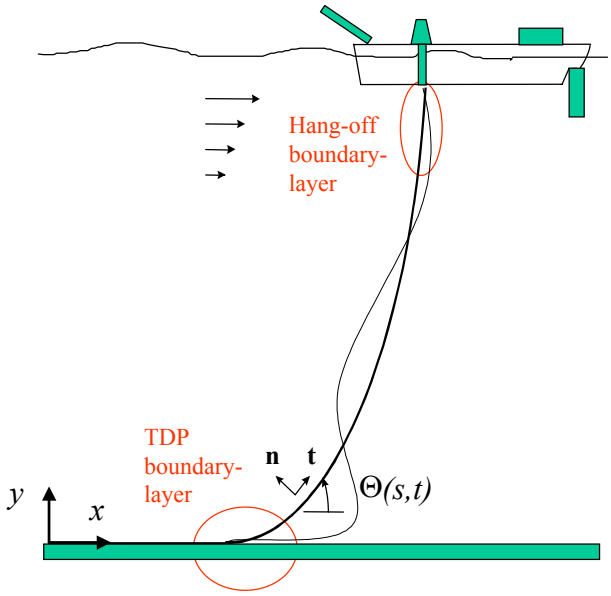

Figure 7.7: The Dynamic Problem and hot spots in a free-hanging catenary riser. Displacements are exaggerated.

Dynamic equilibrium leads to

$$\begin{aligned} &\frac{\partial \mathrm{T}}{\partial s}-\left(\mathrm{T}\gamma+\mathrm{Q}\right)\frac{d\theta}{ds}-\frac{\partial}{\partial s}\left(\mathrm{Q}\gamma\right)+c_t+\varpi_t-qsen\theta=m\frac{\partial^2 u_t}{\partial t^2} \\ &\frac{\partial \mathrm{Q}}{\partial s}+\left(\mathrm{T}-\mathrm{Q}\gamma\right)\frac{d\theta}{ds}+\frac{\partial}{\partial s}\left(\mathrm{T}\gamma\right)+c_n+\varpi_n-q\cos\theta=m\frac{\partial^2 u_n}{\partial t^2}\ . \end{aligned} \tag{7.27}$$

In eqn (7.27), $\varpi_{t,n}(s,t)$ represent the dynamic parcels of the hydrodynamic forces acting on the line, per unit length, due the relative motion with respect to the current and wave flow; see, e.g., Sarpkaya (2001) for a discussion on the subject. Note that eqns (7.27) are coupled through static curvature. By using eqn (7.25), isolating in eqn (7.29) the static equilibrium, eqn (7.1), and neglecting second-order terms, the following dynamic equations around the static configuration can be obtained,

$$\begin{aligned} &\frac{\partial \tau}{\partial s}-\left(T\gamma+\vartheta\right)\frac{d\theta}{ds}-\frac{\partial}{\partial s}\left(Q\gamma\right)+\varpi_t=m\frac{\partial^2 u_t}{\partial t^2} \\ &\frac{\partial \vartheta}{\partial s}+\left(\tau-Q\gamma\right)\frac{d\theta}{ds}+\frac{\partial}{\partial s}\left(T\gamma\right)+\varpi_n=m\frac{\partial^2 u_n}{\partial t^2}\ . \end{aligned} \tag{7.28}$$

7.3.1 The extensible string equations

By using standard constitutive relations, a complete set of equations, including bending-stiffness effects, could be easily deduced. Nevertheless, as pointed out, flexural-rigidity effects are significant just close to the extremities, at least in the

free-hanging catenary case, being the global dynamics dominated by the geometric rigidity. The chosen path is, therefore, to consider just axial and geometric rigidities, correcting the local bending-stiffness effects a posteriori, via boundary-layer techniques. Let *EA* be the axial rigidity. As the dynamic tension can be written as $\tau(s,t) = EAe(s,t)$, the following set of dynamic equations is obtained,

$$\begin{aligned}
&\frac{\partial \tau}{\partial s} - \gamma T \frac{d\theta}{ds} = -\varpi_t + m\frac{\partial^2 u_t}{\partial t^2} \\
&\tau \frac{d\theta}{ds} + \frac{\partial}{\partial s}(\gamma T) = -\varpi_n + m\frac{\partial^2 u_n}{\partial t^2} \\
&\frac{\partial u_t}{\partial s} - u_n \frac{d\theta}{ds} = e \\
&\frac{\partial u_n}{\partial s} + u_t \frac{d\theta}{ds} = (1+\varepsilon)\gamma \\
&e = \frac{\tau}{EA} \quad .
\end{aligned} \tag{7.29}$$

7.3.2 The principle of virtual work

Let (q_t, q_n) be the total (applied and inertial) forces in the tangential and normal directions, respectively, such that $q_t = -\varpi_t + m\partial^2 u_t / \partial t^2$ and $q_n = -\varpi_n + m\partial^2 u_n / \partial t^2$. Let $(\delta u_t, \delta u_n)$ be virtual displacements. Following standard procedures, the principle of virtual work applied to the present problem, with $\delta u_n(0) = \delta u_t(L) = \delta u_n(L) = 0$, leads to

$$\begin{aligned}
&-\int_0^L EA\frac{\partial u_t}{\partial s}\frac{\partial \delta u_t}{\partial s}ds + \int_0^L EA\frac{d\theta}{ds}u_n\frac{\partial \delta u_n}{\partial s}ds \\
&-\int_0^L \frac{T}{1+\varepsilon}\frac{d\theta}{ds}\frac{\partial u_n}{\partial s}\delta u\, ds - \int_0^L \frac{T}{1+\varepsilon}\left(\frac{d\theta}{ds}\right)^2 u_t \delta u_t\, ds \\
&+\int_0^L EA\frac{d\theta}{ds}\frac{\partial u_t}{\partial s}\delta u_n\, ds - \int_0^L EA\left(\frac{d\theta}{ds}\right)^2 u_n \delta u_n\, ds \\
&-\int_0^L \frac{T}{1+\varepsilon}\frac{\partial u_n}{\partial s}\frac{\partial \delta u_n}{\partial s}ds - \int_0^L \frac{T}{1+\varepsilon}\frac{d\theta}{ds}u_t\frac{\partial \delta u_n}{\partial s}ds \\
&+\int_0^L q_t \delta u_t ds + \int_0^L q_n \delta u_n ds - \tau(0)\delta u_t(0) = 0 \quad .
\end{aligned} \tag{7.30}$$

7.3.2.1 Boundary conditions at TDP

At the TDP, $s = 0$, a consistent linearized boundary condition that allows the part of the line that is in contact with the soil to stretch (under a Coulomb friction force with a coefficient μ) and simultaneously imposes a non-detaching condition, may be written,

$$\begin{aligned} &\tau(0,t) = \frac{EA}{\ell'} u_t(0,t) \\ &u_n(0,t) = 0 \end{aligned} ; \tag{7.31}$$

where $\ell' = \max\{\ell_1, \ell_2\}$, being $\ell_1 = \dfrac{T(0)}{\mu q}$ and $\ell_2 = \ell_t - L$.

It should be mentioned that the stretching is mandatory, otherwise the tension would experience large peak values related to the tensioning-wave reflection at the hinge. The proper and complete way to account for the TDP dynamic variation must consider the local bending-stiffness effect, which can be done by applying boundary-layer techniques, as will be shown in section 7.3.6.

7.3.2.2 Boundary conditions at hang-off

If we take a harmonic motion imposed by the floating unit, such that, $\tilde{x}(L,t) = A\cos(\omega t + \varphi_x); \tilde{y}(L,t) = B\cos(\omega t + \varphi_y)$, then,

$$\begin{aligned} &u_t(L,t) = \mathrm{Re}\left[U_t e^{i\omega t}\right] \\ &u_n(L,t) = \mathrm{Re}\left[U_n e^{i\omega t}\right] \end{aligned} , \tag{7.32}$$

where, $U_{t,n} = U_{t,n}^{(c)} + iU_{t,n}^{(s)}$, are easily deduced.

7.3.3 Finite-element method discretization

Let $\Delta_j = s_j - s_{j-1}$, $u_j = u(s_j)$ and $v_j = v(s_j)$; $j = 0,...,n$, with $j = 0$ the TDP. Let also, as usual, $\phi(s,t) = \sum_{j=0}^{n} f_j(s)\,\phi_j(t)$ be any interpolated field. Equations (7.30) indicate that it is sufficient that $f_j(s)$ be linear interpolating functions.

Let also $\mathbf{q} = \left(\mathbf{u}_t \quad \mathbf{u}_n\right)^T$ and **p** be, respectively, the displacement and load vectors and **M**, **C**, and **K** be the mass, (linearized) damping and stiffness matrices. Then eqn (7.30) may be easily written in the discrete and usual form, under harmonic excitation.

$$\mathbf{M}\ddot{\mathbf{q}} + \mathbf{C}\dot{\mathbf{q}} + \mathbf{K}\mathbf{q} = \mathbf{p} . \tag{7.33}$$

In the following we consider $\varepsilon << 1$ in eqn (7.30).

7.3.3.1 The mass matrix

The matrix of mass is simply given by

$$\mathbf{M} = \begin{bmatrix} \mathbf{M}_{nn} & \mathbf{0} \\ \mathbf{0} & \mathbf{M}_{tt} \end{bmatrix}, \tag{7.34}$$

where

$$\left[M_{nn}\right]_{i,j} = \int_0^L m_n f_i f_j ds \;; \quad \left[M_{tt}\right]_{i,j} = \int_0^L m_t f_i f_j ds \,. \tag{7.35}$$

If no strakes are considered, $m_n = \mathrm{m} + c_m \rho_w S$ and $m_t = m$, where c_m is Morison's inertia coefficient. Note that this coefficient is, in fact, at least dependent on the Keulegan-Carpenter number, implying an iterative solution for eqn (7.33). Moreover, if VIV occurs, inertia and drag force coefficients are also function of the current (reduced) velocity; see, e.g., Vikestad et al. (2000). If strakes are considered, inertia coefficient in both normal and tangential directions must be properly accounted for; Lambrakos et al. (2002).

7.3.3.2 The stiffness matrix

As flexural rigidity has been not considered, the stiffness matrix has only the contributions of axial and geometric rigidity matrices, **E** and **G**, respectively, such that,

$$\mathbf{K} = \mathbf{E} + \mathbf{G}$$

$$\mathbf{K} = \begin{bmatrix} \mathbf{K}_{nn} & \mathbf{K}_{nt} \\ \mathbf{K}_{tn} & \mathbf{K}_{tt} \end{bmatrix}. \tag{7.36}$$

It will be clear that $\mathbf{K}_{nt} = \mathbf{K}_{tn}^{\,T}$.

The elastic stiffness matrix (axial rigidity)

The elastic stiffness matrix, due to the axial rigidity, may be written,

$$\mathbf{E} = \begin{bmatrix} \mathbf{E}_{nn} & \mathbf{E}_{nt} \\ \mathbf{E}_{tn} & \mathbf{E}_{tt} \end{bmatrix}, \tag{7.37}$$

where,

$$[E_{nn}]_{i,j} = \int_0^L EA\left(\frac{d\theta_e}{ds}\right)^2 f_i f_j ds; \quad [E_{nt}]_{i,j} = -\int_0^L EA\frac{d\theta}{ds} f_i \frac{df_j}{ds} ds$$

$$[E_{tn}]_{i,j} = -\int_0^L EA\frac{d\theta}{ds}\frac{df_i}{ds} f_j ds \qquad [E_{tt}]_{i,j} = \int_0^L EA\frac{df_i}{ds}\frac{df_j}{ds} ds + \frac{EA}{\ell'} f_i(0) f_j(0) \,, \tag{7.38}$$

where the last term in eqn (7.38), is related to the boundary condition eqn (7.31a) and corresponds to the last term in eqn (7.30).

The geometric stiffness matrix

The geometric stiffness matrix, due to tension, may be written,

$$\mathbf{G} = \begin{bmatrix} \mathbf{G}_{nn} & \mathbf{G}_{nt} \\ \mathbf{G}_{tn} & \mathbf{G}_{tt} \end{bmatrix}, \tag{7.39}$$

where,

$$[G_{nn}]_{i,j} = \int_0^L T \frac{df_i}{ds}\frac{df_j}{ds} ds; \qquad [G_{nt}]_{i,j} = \int_0^L T \frac{d\theta}{ds}\frac{df_i}{ds} f_j \, ds$$
$$[G_{tn}]_{i,j} = \int_0^L T \frac{d\theta}{ds} f_i \frac{df_j}{ds} ds; \quad [G_{tt}]_{i,j} = \int_0^L T\left(\frac{d\theta}{ds}\right)^2 f_i f_j \, ds \; . \tag{7.40}$$

7.3.3.3 The linearized hydrodynamic damping matrix

The linearized hydrodynamic damping matrix is constructed based on a normal approach in ocean engineering. This procedure considers that the energy lost per cycle due to linear damping in velocity is equal to that corresponding to a quadratic law. This renders the solution of the problem iterative, as the coefficients depend on the velocity amplitudes that are not known *a priori*. The linearized damping matrix may be written,

$$\mathbf{C} = \begin{bmatrix} \mathbf{C}_{nn} & \mathbf{0} \\ \mathbf{0} & \mathbf{C}_{tt} \end{bmatrix} \; , \tag{7.41}$$

where

$$[C_{nn}]_{i,j} = \int_0^L c_{nL} f_i f_j ds \; ; \quad [C_{tt}]_{i,j} = \int_0^L c_{tL} f_i f_j ds \tag{7.42}$$

with

$$c_{nL} = \frac{4}{3\pi} \rho_w D c_{d,n} \omega A_0 \; ; \quad c_{tL} = \frac{4}{3\pi} \rho_w D c_{d,t} \omega A_0 \tag{7.43}$$

the linearized damping coefficients, where ω is the frequency of oscillation and A_0 is an integral averaged amplitude of motion calculated along the riser span, as presented in section 7.3.5.

7.3.3.4 The load vector due to wave action along the riser

As hydrodynamic inertia forces and viscous current forces are already included in the matrices of mass and damping, the load vector **p** is, apart from the extremities, considered solely dependent on the direct wave action on the riser span. Hence,

$$\mathbf{p} = [\mathbf{p}_n \quad \mathbf{p}_t]^T \; , \tag{7.44}$$

with,

$$\{p_n\}_i = \int_0^L \overline{a}_w f_i ds \; ; \quad \{p_t\}_i = 0 \; , \tag{7.45}$$

where, $\overline{a}_w(s)$, the wave force per unit length, is obtained from the classical linear free surface wave potential theory. Restricting ourselves to the deep-water case,

$$\bar{a}_w(s) = \frac{4}{3\pi}\rho_w D c_{d,n}\omega^2 A_w^2 S_w e^{k_w(y(s)-H)}\{[\cos(S_w k_w x(s)) - i\sin(S_w k_w x(s))] \\ [-\sin(S_w\theta(s)) + i\cos(S_w\theta(s))]\}. \tag{7.46}$$

In eqn (7.46), $k_w = \omega^2/g$ is the wave number in deep water, A_w the wave amplitude and $S_w = \pm 1$, according to the wave-propagation direction, positive if pointing towards the horizontal axis x.

7.3.4 Frequency-domain solution

Consider the harmonic problem, the solution being $\mathbf{q(t)} = \mathbf{q_0}e^{i\omega t}$. Equation (7.33) reads

$$\begin{aligned} &\mathbf{D}\mathbf{q}_0 = \mathbf{p}_0 \\ &\mathbf{D} = \left[-\omega^2\mathbf{M} + i\omega\mathbf{C} + \mathbf{K}\right], \end{aligned} \tag{7.47}$$

where $\mathbf{D}$ is the dynamic matrix. The displacement $\mathbf{q_0}$ and the corresponding load vector can be reordered as

$$\mathbf{q}_0 = \begin{Bmatrix}\mathbf{q}_1 \\ \mathbf{q}_2\end{Bmatrix}; \quad \mathbf{p}_0 = \begin{Bmatrix}\mathbf{p}_1 \\ \mathbf{p}_2\end{Bmatrix}, \tag{7.48}$$

where $\mathbf{q}_1$ corresponds to the constraints, $\mathbf{p}_1$ being the associated unknown applied forces and $\mathbf{q}_2$ the unknown displacements. Accordingly,

$$\mathbf{D} = \begin{bmatrix}\mathbf{D}_{11} & \mathbf{D}_{12} \\ \mathbf{D}_{21} & \mathbf{D}_{22}\end{bmatrix}. \tag{7.49}$$

Then, eqn (7.47) can be written

$$\begin{aligned} &\mathbf{D}_{11}\mathbf{q}_1 + \mathbf{D}_{12}\mathbf{q}_2 = \mathbf{p}_1 \\ &\mathbf{D}_{22}\mathbf{q}_2 = \mathbf{p}_2 - \mathbf{D}_{21}\mathbf{q}_1. \end{aligned} \tag{7.50}$$

Once eqn (7.50b) is solved, given $\mathbf{p}_2$ and $\mathbf{q}_1$, eqn (7.50a) determines the constraining forces $\mathbf{p}_1$. This is accomplished by taking, in accordance with eqns (7.31b) and (7.32),

$$\mathbf{q}_1 = \begin{pmatrix}0 & U_n & U_t\end{pmatrix}^t. \tag{7.51}$$

The axial displacement at TDP, boundary condition eqn (7.31a), is already considered in the stiffness matrix.

7.3.5 Hydrodynamic damping linearization

Hydrodynamic damping obeys a quadratic law in relative velocities. Let $v_{r,n}(s) = \omega\, A_n(s)\sin\omega t$ represent the relative normal velocity along the riser. Note that $A_n(s)$ is, *a priori*, unknown and will be determined at each step of the iterative solution in frequency domain. Let A_0 be the integral averaged amplitude along the riser. By equating the dissipated energy per cycle

$\int_0^{\ell}\int_0^{T} f_{d,n} v_{r,n}\, dt\, ds = \int_0^{\ell}\int_0^{T} \widetilde{f}_{d,n} v_{r,n}\, dt\, ds$, A_0 can be calculated. Two cases are considered: (i) only waves act, current being absent; (ii) wave is considered as well, but current dominates the velocity field.

In the first case, $v_{r,n} = \frac{\partial u_n}{\partial t} - v_{w,n}$, where v_w refers to the wave-field velocity, such that $f_{d,n}(s) = -1/2\, \rho_w D\, c_{d,n}\, \omega^2 A_n^2(s) \left|\sin \omega t\right| \sin \omega t$ and $\widetilde{f}_{d,n}(s) = -4/3\pi\ \rho_w D\, c_{d,n}\, \omega^2 A_0\ A_n(s) \sin \omega\, t$. This leads to,

$$A_0 = \frac{\int_0^L A_n^3(s) ds}{\int_0^L A_n^2(s) ds}. \tag{7.52}$$

In the second case, $v_{r,n} = \frac{\partial u_n}{\partial t} - v_{w,n} - v_{c,n}(s)$. Considering current as dominant, i.e., taking $v_{c,n}(s) >> \frac{\partial u_n}{\partial t} - v_{w,n}$, the dynamic parcel of the nonlinear force is given by $f_{d,n}(s) = -\rho_w\, D\, c_{d,n} \left|v_{c,n}(s)\right| \omega\ A_n(s) \sin \omega\, t$, whilst the linearized viscous force takes the form $\widetilde{f}_{d,n}(s) = -4/3\pi\ \rho_w\, D\, c_{d,n}\, \omega^2\ A_0\ A_n(s) \sin \omega\, t$, which leads to

$$A_0 = \frac{3\pi}{4\omega} \frac{\int_0^L \left|v_{c,n}(s)\right| A_n^2(s)\, ds}{\int_0^L A_n^2(s)\, ds}. \tag{7.53}$$

7.3.6 The flexural-rigidity effect at extremities

The numerical solution in the frequency domain was obtained by disregarding flexural-rigidity effects and by linearizing the boundary conditions at extremities. Particularly, the TDP was considered as a hinge that can move horizontally, constrained by a linear spring. This solution *must* be corrected in the TDP and hang-off boundary layers, where the flexural-rigidity effect is not negligible any longer. For the TDP analysis, the soil is firstly supposed to be infinitely rigid. The effect of finite rigidity is then incorporated.

7.3.6.1 Sub-critical dynamic boundary-layer solution in the TDP region: rigid soil.

Under the ideal-cable assumption, motivated by an earlier work of Burridge et al. (1982), Triantafyllou et al. (1985) showed that a shock condition in which the cable impacts the soil would hold whenever the local 'Mach' number,

$\mathrm{M} = \dot{x}_0 / c_0 \geq 1$. Here $x_0(t)$ is the function describing the instantaneous position of the TDP, $c_0 = \sqrt{T_0/(m+m_a)}$ is the local cable wave celerity and T_0 is the local static tension. This assertion can be physically interpreted as the lack of time for the cable to adjust its geometric form. Conversely, the condition $\mathrm{M} < 1$ is said to be a *sub-critical dynamic regime.* For this latter situation, it has also been shown that *the inertia term can be locally disregarded*, with an error of the order of $\mathrm{M}^2 << 1$; Aranha et al. (1997). Moreover, in the sub-critical regime, the boundary condition for the global quasi-linear equation can be taken as a simple hinge, placed at the cable static TDP with an error of order $O\left(a_0 \chi_0\right)^2$, where a_0 is the typical amplitude of $x_0(t)$ and $\chi_0 = q/T_0$, the local cable curvature.

Recalling (Aranha et al. (1993); Aranha and Pinto (2001)) that, at least close to the TDP, the dynamic tension is weakly varying along the arc length, we write $\tau(0,t) = \tau(t)$ as the local dynamic tension. Let $\xi = s/\lambda$ and $f(t) = 1 + \tau(t)/T_0$ be the local nondimensional static coordinate and total tension. We assume that the condition $f(t) > 0$ holds, precluding compression. A boundary-layer solution is then found, Aranha et al. (1997), with an error of order $O(\mathrm{M}^2 << 1)$, as

$$\frac{\chi(\xi,t)}{\chi_0} = \begin{cases} \dfrac{1}{f(t)}\left(1 - \exp\left(-\beta(\xi,t)\right)\right); & \text{if } \beta(\xi,t) > 0 \\ \text{or} & \\ 0; \text{ if } & \beta(\xi,t) \leq 0 \end{cases}$$

with (7.54)

$$\beta(\xi,t) = \sqrt{f(t)}\left(\xi - \xi_f(t)\right) = \sqrt{f(t)}\left(\xi - \xi_0(t)\right) + 1 \ .$$

This is valid for a rigid soil, recovering the static solution, for which $\tau(t) = x_0(t) \equiv 0$. All global static information, including the global effect of current, is contained in the static parameter T_0, so in $\chi_0 = q/T_0$. All global dynamic information is locally represented by the functions $\tau(t)$ and $x_0(t)$, which can be numerically calculated. In eqn (7.54), $\xi_f(t) = \xi_0(t) - 1/\sqrt{f(t)}$ is the actual TDP instantaneous position, including flexural rigidity effects and measured from the static 'ideal cable' TDP. The non-linear boundary-layer solution does not depend on the particular form taken by the oscillatory (global) functions $f(t)$ and $\xi_0(t)$ and can be easily applied to a response analysis under random excitation.

The analytical boundary-layer solution for the curvature was verified experimentally. A rod, properly scaling the boundary layer region of a SCR, was instrumented with an array of 100 strain-gauges. Figure 7.8 shows an example comparing the asymptotic solution with experimental results. The normalized curvature is shown as a function of time for the critical section, where the curvature variation attains a maximum value.

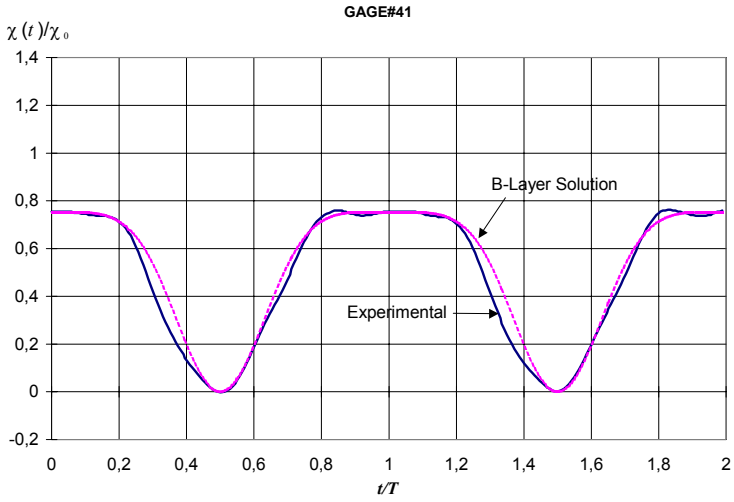

Figure 7.8: Nondimensional curvature $\chi(t)/\chi_0$. "Critical section", Pesce et al. (1998a). $\chi_0 = q/T_0 = 0.0409m^{-1}$; $a_0/\lambda = 1.1619$; $s/\lambda = 0.0435$; $\tau_0/T_0 = 0.2004$; $\varphi = \pi$; $M = 0.055$.

Figure 7.9 shows a comparison between the TDP boundary-layer solution with the results obtained with a non-linear code run in the time domain, for a 16" diameter SCR, in 575 m deep water. Only a circular motion was imposed at the top end, with an amplitude of 0.2 m. The period of excitation was 7.8 s. This condition corresponds to the motion of a semi-submersible platform in a typical sea-state in Campos Basin (Brazil). The agreement is very good.

Note that a *clockwise* or an *anti-clockwise* motion led to different results, particularly for the RMS curve. The cause of this is the global effect of the iterative solution obtained by linearizing the viscous damping along the riser, the only source of nonlinearity in the global dynamics. The sense of rotation imposed on the top affects the dynamic tension $\tau(t)$ and the TDP excursion $x_0(t)$, both in amplitude and relative phases and hence, the curvature $\chi(t)$.

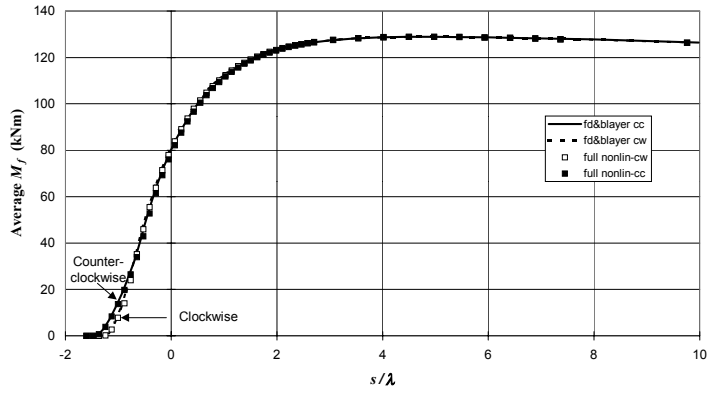

(a)

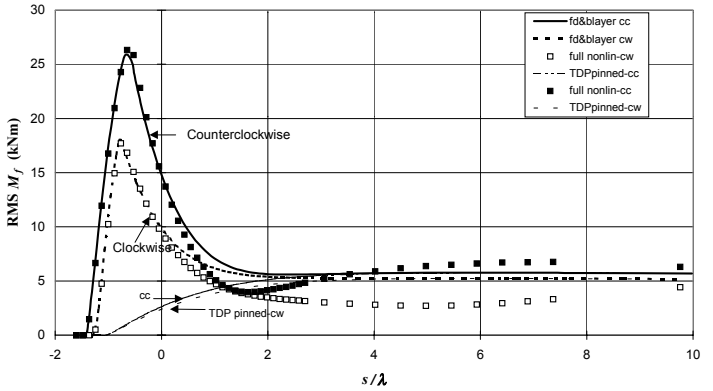

(b)

Figure 7.9: Average and RMS values of the bending moment in the vicinity of the touchdown point for a 16" SCR, as a function of s/λ . Comparing a frequency-domain solution corrected with the boundary-layer technique, with a nonlinear time-domain simulation (Aranha et al. (1997)).

7.3.6.2 Sub-critical dynamic boundary-layer solution in the TDP region: linear elastic soil.

The result presented in section 7.2.3.2 can be extended to a sub-critical dynamic regime, i.e., under the hypothesis of no impact against the soil, in a quasi-static manner, as that presented in the previous section. A proper time-scales analysis shows that for many typical cases may be treated as if as the local sub-critical dynamics were governed by the global dynamics of the suspended part. Details

may be found in Pesce & Martins (2004). Let, as before, $\xi = s/\lambda$ and $f(t) = 1 + \tau(t)/T_0$ be nondimensional quantities. Let also $X_0 = \chi_0 \lambda$ be the nondimensional catenary curvature at the TDP. The local elastica may be shown to be,

$$\eta(\xi,t) = \frac{X_0}{\sqrt{f(t)}} \frac{\sqrt{2}}{K^{1/2}} \frac{1}{K^{1/4} + \sqrt{2 f(t)}} \exp\left(\frac{K^{1/4}}{\sqrt{2}} (\xi - \xi_f(t)) \right) \times \\ \times \sin\left(\frac{K^{1/4}}{\sqrt{2}} (\xi - \xi_f(t)) \right)$$

$$\text{valid for } \left(\xi - \xi_f(t)\right) \le 0 \text{ , i.e, on the soil, and} \tag{7.55}$$

$$\eta(\xi,t) = \frac{X_0}{f(t)} \left\{ \frac{\xi^2 - \xi_f^2(t)}{2} - \xi_0(t)\left(\xi - \xi_f(t)\right) \right\} + \\ + \frac{X_0}{f(t)} \left\{ \frac{1}{f(t)} \frac{K^{1/4}}{K^{1/4} + \sqrt{2 f(t)}} \left[1 - \exp\left[- \sqrt{f(t)} \left(\xi - \xi_f(t)\right) \right] \right] \right\}$$

$$\text{valid for } \left(\xi - \xi_f(t)\right) \ge 0 \text{ , i.e., along the suspended part.}$$

where

$$\xi_f(t) = \xi_0(t) - \frac{K^{1/4}}{K^{1/4} + \sqrt{2 f(t)}} \left(\frac{1}{\sqrt{f(t)}} - \frac{\sqrt{f(t)}}{K^{1/2}} \right) \tag{7.56}$$

is the instantaneous nondimensional position of the TDP, measured with respect to the static position of the equivalent ideal cable TDP and defined such that $\eta(\xi_f(t), t) \equiv 0$. The angle with respect to the horizontal, the nondimensional curvature and the shear force are readily deducible from eqn (7.55). Equation (7.55) recovers both limit cases: the static case on linear elastic soil and the sub-critical dynamic case on rigid soil.

Figures 7.10 and 7.11 show local analytical solutions for the normalized elastica, angle, curvature and shear. Snapshots along a half cycle of harmonic excitation are presented. For simplicity, TDP excursion is taken as $\xi_0(t) = x_0(t)/\lambda = a_0 \cos\omega t$ and the dynamic tension function, in anti-phase, such that $f(t) = 1 - \tau_0(t)/T_0 = 1 - \beta_0 \cos\omega t$.

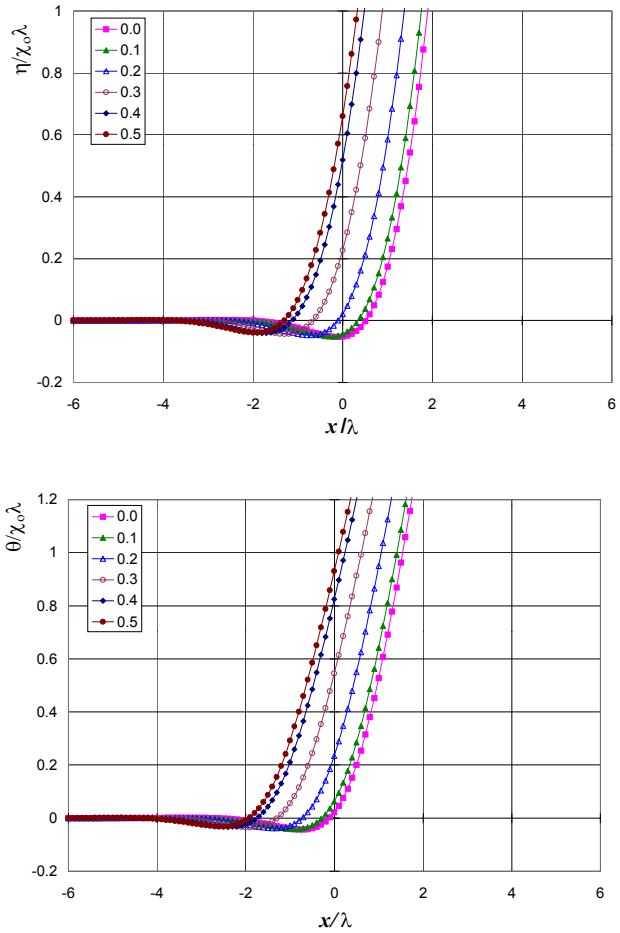

Figure 7.10: Local normalized, (a) elastic curve and (b) angle with respect to the horizontal. Soil rigidity parameter: $K = 10$. Snapshots for $t/\mathrm{T} = 0;\ 0.1;\ 0.2;\ 0.3;\ 0.4;\ 0.5;\ \ \mathrm{T} = 2\pi\omega^{-1};\ a_0 = 1; \beta_0 = 0.2$. Pesce & Martins (2004).

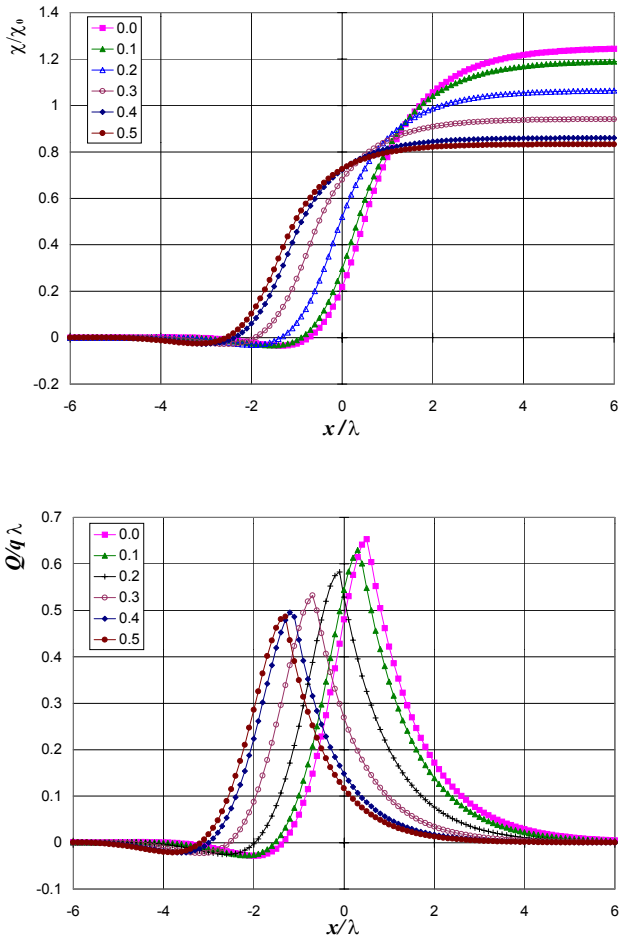

Figure 7.11: Local normalized (a) curvature and (b) shear force. Soil rigidity parameter: $K = 10$. Snapshots for $t/\mathrm{T} = 0;\ 0.1;\ 0.2;\ 0.3;\ 0.4;\ 0.5;$ $\mathrm{T} = 2\pi\omega^{-1};\ a_0 = 1; \beta_0 = 0.2$. Pesce & Martins (2004).

The soil is considered to be relatively soft, with $K = 10$. Observe that, at a given section x/λ, angle, curvature and shear vary cyclically, while the TDP position oscillates, forcing the riser to penetrate into the linear elastic soil, as seen in Figure 7.10. The variation observed in the shear-force peak is due to the oscillation in the dynamic tension, for this particular choice of amplitude and phase.

7.3.6.3 The boundary-layer solution at the top end

Using a similar reasoning, see Pesce (1997) or Martins (2000), applied to the top end, leads to the following boundary-layer solution for the curvature at the upper region,

$$\chi(s,t) = \chi^c(s,t) - \frac{1}{\lambda_L}\left(\chi_L^c(t)\lambda_L + \frac{k_F\lambda_L}{B}\left(\Theta_L(t) - \Phi(t)\right)\right)e^{\left(\sqrt{1+\frac{\tau(t)}{T_L}}\frac{s-L}{\lambda_L}\right)}, \qquad (7.57)$$

where the angle at the top is given by,

$$\Theta_L(t) = \frac{\Theta_L^c(t) + \dfrac{1}{\sqrt{1+\tau(t)/T_L}}\left(\dfrac{k_F\lambda_L}{B}\Phi(t) - \chi_L^c(t)\lambda_L\right)}{1 + \dfrac{k_F\lambda_L}{B}\dfrac{1}{\sqrt{1+\tau(t)/T_L}}}. \qquad (7.58)$$

In eqns (7.57) and (7.58), $\lambda_L = \sqrt{EI/T_L}$ is the local 'flexural length' at top; T_L is the static tension and θ_L is the static angle at the upper end; $\chi^c(s,t)$ is the dynamic ideal cable curvature; $\tau(t)$ is the local dynamic tension; $\Phi(t)$ is the angle, with respect to the horizontal imposed by the floating unit to the cable; k_F is the flexural rigidity for a unitary angle rotation corresponding to a *linear* flexible top connection. We should expect some non-linear behaviour only for large values of the dynamic tension amplitude. The static solution can be readily determined from the above equations, as a particular case.

Figure 7.12 presents the dynamic amplitude of curvature, comparing the boundary-layer analytical solution with a full non-linear numerical solution obtained with a numerical code. The agreement is very good. For reference, the curve corresponding to the ideal catenary is also presented. It is clear that the flexural boundary layer has a length of about $4\lambda_L$, 18.4 meters in this case.

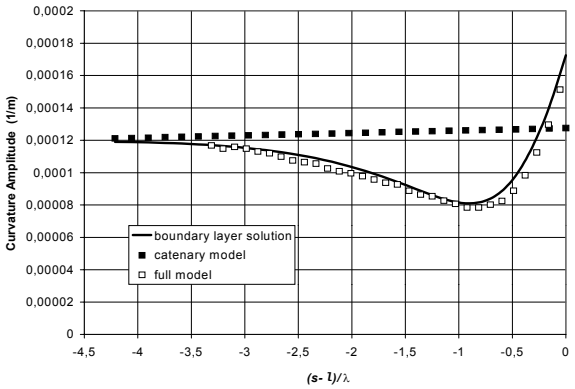

Figure 7.12: Dynamic amplitude of curvature at top, for a SCR $k_F = 10\,\text{kN/degree};\ \lambda_L = 4.60\,\text{m};\ L = 970\,\text{m}$. Asymptotics compared to a full nonlinear code; Martins et al. (2000).

7.3.7 The planar eigenvalue problem

The discrete linear formulation in the frequency domain enables us to numerically solve the associate eigenvalue problem in an easy way. This section recovers an analytical approximation for the eigenvalue problem, aiming to enlighten the discussion a little further and to serve as a basis for comparison with numerical calculations.

For simplicity, we neglect geometrically and dynamically nonlinear terms, considering only the case of a non-extensible and infinitely flexible (*EI*=0) line (an ideal heavy cable). We point out that ignoring axial deformation, being physically inadequate, leads to a mathematical ill-posedeness, since axial boundary conditions cannot be properly enforced any longer. A complete and more proper account of this subject is given, for small sagged cables, by Irvine and Caughey (1974) and, for marine cables, by Triantafyllou (1984).

According to Triantafyllou (1984), "in the case of a taut wire, stretching is of second order, but the elastic stiffness must be finite, otherwise is geometrically impossible to have any vibrations at all. In the case of a sagging cable the elastic stiffness can be infinite, because the cable admits transverse displacements causing second-order tangential displacements by readjusting its curvature and with no stretching". Triantafyllou considers two basic asymptotic solutions. The first one is slightly varying in space[3], compared to the static tension, stretching being mandatory. This solution is given in terms of Airy functions. The dynamic tension is also slightly varying in space and strongly dependent on elastic stiffness (axial rigidity). The second solution is highly varying in space and given as a WKB approximate solution, consistent with assuming an infinite elastic stiffness, i.e., a non-extensible wire. The total solution is a linear combination of both. In the slightly varying solution, elastic stiffness dominates the upper part and curvature the lower part. This fact causes modes to be hybrid, neither symmetric nor anti-symmetric. In fact, a turning point close to the upper end exists in the Airy function solution.

Define $\xi = s/L$, $\upsilon = u_t/L$, $\eta = u_n/L$ and $\hat{t} = t\,c_0/L$ as non-dimensional (global) quantities. Let $\upsilon(\xi,t) = \psi(\xi)e^{i\hat{\omega}\hat{t}}$ and $\eta(\xi,t) = \varphi(\xi)e^{i\hat{\omega}\hat{t}}$, $\hat{\omega} = \omega\, L/c_0$. If viscous and quadratic terms in curvature are neglected the planar linear eigenvalue problem can be written, Pesce et al. (1999),

$$\begin{aligned} &\psi(\xi) = \hat{\omega}^{-2}\left[(1+a)F(\xi)\chi(\xi)\right]\varphi'(\xi) \\ &\left(F(\xi)\varphi'\right)' + \hat{\omega}^2\varphi = 0 \end{aligned} \tag{7.59}$$

where $a = m_a/m$ is here defined as the added mass coefficient[4] and

$$F(\xi) = T(\xi)/T_0 = \left(c(\xi)/c_0\right)^2 \tag{7.60}$$

is the nondimensional effective tension function; $c(\xi) = \sqrt{T(\xi)/(m+m_a)}$ is the local transversal wave celerity for a cable.

---

[3] Triantafyllou uses the terms 'slowly' and 'fast' varying in space.

[4] Usually $C_m = m_a/m_d$, where m_d is the displaced mass.

Equation (7.59b) is, strictly speaking, the eigenvalue equation. Equation (7.59a) gives the tangential displacement $\psi(\xi)$, as a direct linear operation on $\varphi(\xi)$, a consequence of not considering extensibility, which is a real drawback of the present analysis. Also, depending on the actual value taken by the non-dimensional axial-to-geometric-ratio rigidity parameter, as defined by Irvine and Caughey (1974), the hypothesis on non-extensibility can lead to a complete misinterpretation concerning the first eigenmode.

In the particular but important case of a free-hanging and pure catenary (no current) the non-dimensional tension function can be easily shown to be $F_c(\xi) = \sqrt{1+\tan^2\theta_c(\xi)}$, suggesting that we introduce a new variable, $\zeta = \tan\theta(\xi)$.

Therefore, in the pure catenary case, $F_c(\zeta) = \sqrt{1+\zeta^2}$, such that $F_c(\zeta) \approx \zeta$, for $\zeta >> 1$, i.e., in the region close to the upper end, for top angles $\theta_L > \pi/4$, and $F_c(\zeta) \approx 1$ in the TDP region, where $\zeta << 1$. On the other hand, for very low values of θ_L (very tight cables), the tension function can be written $F_c(\zeta) \cong 1 + O(\zeta^2)$. Figure 7.13 shows the tension function $F_c(\zeta)$. This curve is almost linear.

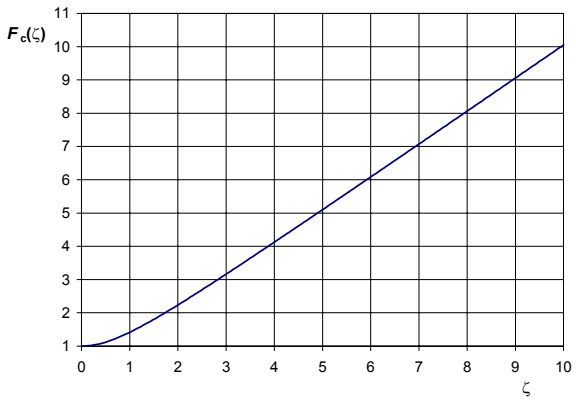

Figure 7.13: Non-dimensional tension function, $F_c(\zeta)$, along a free-hanging (pure) catenary riser.

If a linear approximation (e.g., of the least square type) were taken, a modified Bessel equation would be obtained leading to a classical approximate solution; see, e.g., Bowman (1958). This is straightforward. Instead, given a general $F(\zeta)$, a 'general' closed-form solution, can be easily obtained; Triantafyllou (1984), Pesce et al. (1999). In fact, writing eqn (7.59) as

$$\begin{aligned} &\psi(\zeta) = \Lambda^{-2}(1+a)F(\zeta)\chi(\zeta)\varphi'(\zeta) \\ &\varphi'' + F^{-1}F'\varphi' + \Lambda^2 F^{-1}\varphi = 0 \ , \end{aligned} \tag{7.61}$$

where $\Lambda = \hat{\omega}/\tan\theta_L$, WKB technique (see, e.g., Carrier et al. (1983)), leads to

$$\varphi(\zeta) \cong F^{-1/4}(\zeta)\left[C_1 \sin\left(\Lambda\int^{\zeta} F^{-1/2}(u)du\right) + C_2\cos\left(\Lambda\int^{\zeta} F^{-1/2}(u)du\right)\right], \tag{7.62}$$

a rather general and fairly form, valid not only for the riser-like problem but also for jumpers, for instance. We point out that the determined eigenmodes are sinusoidal functions, modulated in phase and amplitude and resemble Bessel functions. Also, from eqn (7.62), with $\phi(\zeta) = \Lambda\int^{\zeta} F^{-1/2}d\zeta$, the phase angle, the local non-dimensional wave number is given by $\kappa = d\phi/d\zeta = \Lambda/\sqrt{F(\zeta)}$. In other words, $c(\zeta)/c_0 = \Lambda/\kappa$, as should be expected; see, e.g. Whitham (1974), p. 365. If $F(\zeta) = F_0$, a constant, there would be no dispersion at all and eqn (7.59) would be transformed into the classical string equation under constant tension.

Applying, e.g., a pinned-pinned boundary condition, such that, $\varphi(0) = \varphi(\tan\theta_L) = 0$, we get

$$\begin{aligned} \varphi_n(\zeta) &\cong A_n F^{-1/4}(\zeta)\sin\left(\Lambda_n\int_0^{\zeta} F^{-1/2}(u)du\right) \\ \Lambda_n &\cong n\pi\left(\int_0^{\tan\theta_L}\frac{d\zeta}{\sqrt{F(\zeta)}}\right)^{-1} . \end{aligned} \tag{7.63}$$

And the natural frequencies are given by

$$\Omega_n = \Lambda_n \tan\theta_L \frac{c_0}{L} \cong \Lambda_n \tan\theta_L \sqrt{\frac{T_0}{(m+m_a)L}} . \tag{7.64}$$

An important result can be extracted from eqn (7.64): if extensibility is not taken into account, natural frequencies increase linearly with respect to the mode number *n*. This latter observation will be confirmed numerically.

In the case of a *free-hanging and pure catenary riser* (no current), with the tension force given by $F_c(\zeta) = \sqrt{1+\zeta^2}$, we obtain

$$\begin{aligned} \varphi_n(\theta;\theta_L) &\cong A_n(\cos\theta)^{1/4}\sin\left\{\Lambda_n\int_0^{\theta}\frac{d\theta}{(\cos\theta)^{3/2}}\right\} \\ \Lambda_n &= \Lambda_n(\theta_L) \cong \frac{n\pi}{\int_0^{\theta_L}\frac{d\theta}{(\cos\theta)^{3/2}}} . \end{aligned} \tag{7.65}$$

For this particular case it can also be shown that

$$\Omega_n \cong \Lambda_n\sqrt{\frac{(1-\cos\theta_L)}{\cos\theta_L}}\sqrt{\frac{(1-a)}{(1+a)}}\sqrt{\frac{g}{H}} , \tag{7.66}$$

which gives a practical formula for the analytical evaluation of the natural frequencies of a catenary line, written solely in terms of water depth H and of the upper-end angle with respect to horizontal, θ_L .

7.3.7.1 Numerical comparison

The figures below show the WKB approximations for eigenvalues and corresponding eigenmodes for the free-hanging steel catenary riser given in Table 7.1. For simplicity, the riser was supposed to be hinged at TDP and at hang-off, in the absence of current. No flexural rigidity correction was taken into account.

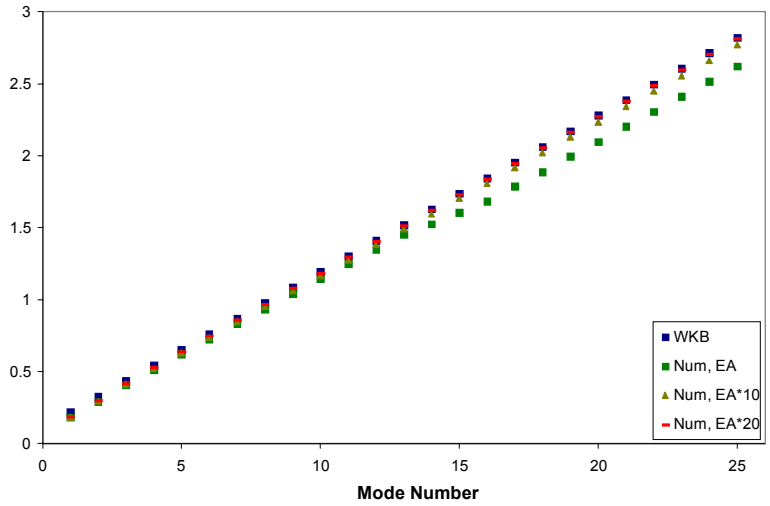

Figure 7.14: Natural frequencies Ω_n (rad/s) of a SCR (Table 7.1). Addressing the extensibility effect. Numerical solution compared to a WKB analytical approximation (the upper square dots).

Solutions are compared to the numerical results, calculated with the presented numerical scheme, by taking the extensibility of the riser into account. In order to address the effect of extensibility, the numerical solution was obtained for three different cases: (i) the nominal EA=2.314E06 kN; (ii) $10\times EA$; (iii) $20\times EA$. Actually it can be verified that the nondimensional parameter that gauges the axial-to-geometric rigidity relative importance, defined by Irvine and Caughey (1974), say $\overline{\Lambda}$, is large in the present analysis, typically of order 20. According to those authors for a similar symmetric case, the first 'symmetric' mode is expected to occur with two internal nodes whenever $\overline{\Lambda} \geq 2\pi$. So, the first numerical eigenmode appeared as an 'anti-symmetric' one. The fundamental mode (no nodes) must, therefore, be disregarded in WKB solution.

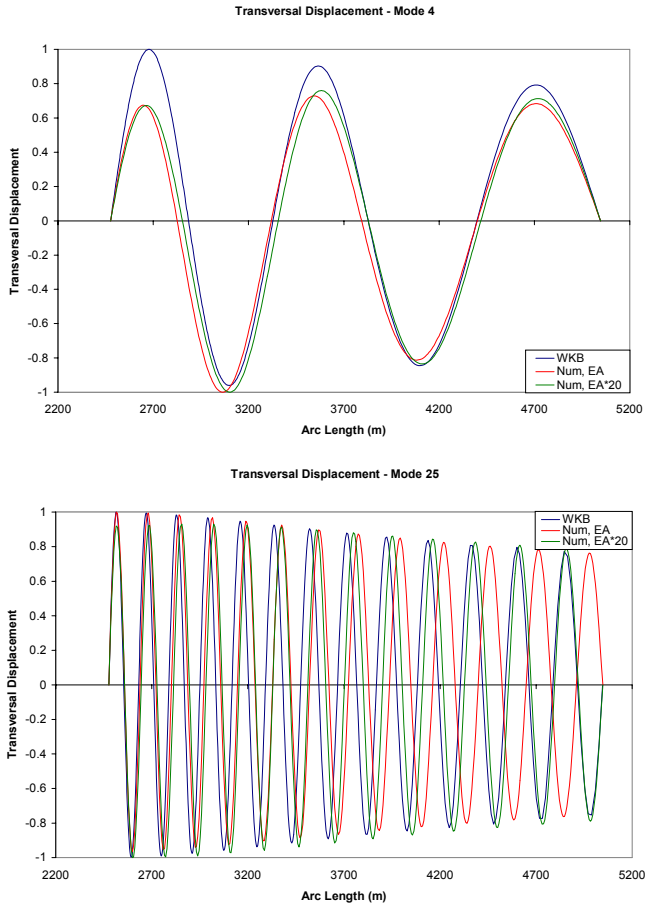

Figure 7.15: WKB approximate solution compared to numerical results obtained by a standard finite-element method. Free-hanging SCR (Table 7.1). $\tan\theta_L = 2.747$. No flexural-rigidity or soil effects are incorporated.

Figure 7.14 presents eigenfrequencies calculated for the installation angle $\theta_L = 70^o$ ($\tan\theta_L = 2.747$), comparing the WKB (non-extensible) solution to numerical results obtained under conditions (i), (ii) and (iii). The agreement is good, particularly for 'low-order' eigenmodes, although, strictly speaking, the WKB technique is applicable for large nondimensional eigenvalues, Λ.

As should be expected, the natural frequency decreases as the axial extensibility increases in the numerical solution. The present WKB approximate solution predicts a linear increase of eigenfrequencies with the mode number. As can be observed, the extensibility effect detaches the curve from the linear behavior. It should be pointed out that if we had considered the effective length laid on the sea floor the extensibility effect would be even more relevant.

Figure 7.15 shows transversal displacements for two eigenmodes. The extensibility effect is assessed numerically; see also Chucheepsakul and Huang

(1997) for a discussion on this subject. Observing mode 25, it can be seen that a very high axial rigidity recovers the WKB asymptotic solution. On the other hand, extensibility decreases the number of nodes that are present in higher modes, as could be expected. For a discussion on soil rigidity effects, see Pesce and Martins (2004).

7.3.8 Time-domain solution

A complete and full nonlinear time-domain simulation should consider the entire system, by taking into account: FPU motions, environmental loading (waves, wind and current) as well as the evolution in time of mass, damping and stiffness matrices. Note that added mass is at least a function of amplitude of motion and current velocity (see, e.g., Sarpkaya (2003)). Damping obeys quadratic laws with respect to relative velocities. Geometric stiffness depends on tension, which is variable with the time. Besides, if any ancillary equipment is present, as strakes for instance, hydrodynamic loads are dependent on geometry and the flow regime; Lambrakos et al. (2002).

For simplicity we shall restrict ourselves to two sources of nonlinearity: damping and the TDP excursion. In other words, the scheme described below is not a full nonlinear method. As a matter of fact, for design purposes, where dynamic displacements are small if compared to the suspended length, such an intermediate methodology proves to be much more efficient. Under these hypotheses the dynamic equations are simply written,

$$\mathbf{M}\ddot{\mathbf{q}} + \mathbf{B}(\dot{\mathbf{q}})\dot{\mathbf{q}} + \mathbf{K}\mathbf{q} = \mathbf{p}(t)\,, \tag{7.67}$$

where,

$$\mathbf{B} = \begin{bmatrix} \mathbf{B}_{nn} & \mathbf{0} \\ \mathbf{0} & \mathbf{B}_{tt} \end{bmatrix} \tag{7.68}$$

$$\begin{aligned} \left[B_{nn}\right]_{i,j} &= \frac{1}{2}\rho_w \int_0^L D(s) c_{d,n}(s)\, f_i(s) f_j(s) \left|\dot{u}_n(s,t) - v_{f,n}(s,t)\right| ds \\ \left[B_{tt}\right]_{i,j} &= \frac{1}{2}\rho_w \int_0^L D(s) c_{d,t}(s) f_i(s) f_j(s) \left|\dot{u}_t(s,t) - v_{f,t}(s,t)\right| ds\,. \end{aligned} \tag{7.69}$$

In eqn (7.69), $v_{f,n,t}$ are the normal and tangential components of the fluid velocity (including waves and current). Note that even the force coefficients are, strictly speaking, functions of relative velocity. Moreover, the suspended length is a function of time. Note also that the load vector includes viscous forces determined at each instantaneous position. As part of the viscous forces is already considered in the second term of eqn (7.67), $\mathbf{B}(\dot{\mathbf{q}})\dot{\mathbf{q}}$, the dynamic loading vector[5] is given by

[5] (the static parcel is already considered in the static solution)

$$\left\{P_{n,t}\right\}_i = \frac{1}{2}\rho_w \int_0^L D(s) c_{d,n,t} f_i(s) \left|\dot{u}_{n,t}(s,t) - v_{f,n,t}(s,t)\right| \cdot v_{f,n,t}(s,t) ds \,. \qquad (7.70)$$

7.3.8.1 Numerical Methods

Explicit or implicit numerical schemes may be applied. Explicit methods typically require less computational effort per time step. Nevertheless, much shorter time steps are often required, making the total computational time larger. Some possibilities may be easily found in the specialized literature (see, e.g., Bathe (1996)): central difference method (CDM), Houlbolt method (HBM), Wilson-Theta method (WTM) and Newmark method (NWM).

A simple ('bench-mark') computer code may be easily written for this specific problem, to address some features, such as: (i) initial procedures, (ii) stability, (iii) accuracy, (iv) flexibility and (v) speed. Table 7.2 presents a qualitative comparison on the above methods; Silveira and Martins (2003).

The Newmark Method presents some advantages. In fact, API-2RD Recommended Practice (1998), page 86, states: "Newmark method is one of the most popular". Initial procedures are not needed, this method is unconditionally stable, presents good accuracy (even when compared to analytical solutions) and good flexibility (by changing the integration parameters). Even though it is not the fastest one, it is not too much slower when compared to simpler methods such as the central difference method.

Table 7.2: Numerical methods; a qualitative comparison; (*** means better evaluation).

	CDM	HBM	WTM	NWM
Initial Procedures	*	*	***	***
Stability	*	***	***	***
Accuracy	**	**	***	***
Flexibility	*	*	**	***
Speed	***	***	*	**

Newmark-method Implementation

An implementation of the Newmark method takes,

$$^{t+\Delta t}\dot{u} = {}^{t}\dot{u} + \left[(1-\delta)\,{}^{t}\ddot{u} + \delta\,{}^{t+\Delta t}\ddot{u}\right]\Delta t \qquad (7.71)$$

$$^{t+\Delta t}u = {}^{t}u + {}^{t}\dot{u}\Delta t + \left[\left(\frac{1}{2}-\alpha\right){}^{t}\ddot{u} + \alpha\,{}^{t+\Delta t}\ddot{u}\right]\Delta t^2 \,, \qquad (7.72)$$

where, Δt is the time step and α and δ are integration parameters. Equation (7.71) can be solved for $^{t+\Delta t}\ddot{u}$ and eqn (7.72) for $^{t+\Delta t}\dot{u}$. Therefore, both $^{t+\Delta t}\ddot{u}$ and $^{t+\Delta t}\dot{u}$ may be written by means of $^{t+\Delta t}u$, and eqn (7.67) is then solved for the time $t + \Delta t$:

$$\mathbf{M}\ {}^{t+\Delta t}\ddot{\mathbf{q}} + \mathbf{B}\ {}^{t+\Delta t}\dot{\mathbf{q}} + \mathbf{K}\ {}^{t+\Delta t}\mathbf{q} = {}^{t+\Delta t}\mathbf{p}\,, \tag{7.73}$$

leading to ${}^{t+\Delta t}u$, ${}^{t+\Delta t}\dot{u}$ and ${}^{t+\Delta t}\ddot{u}$ obtained from ${}^{t}u$, ${}^{t}\dot{u}$ and ${}^{t}\ddot{u}$. The values of the integration parameters must obey the following relations:

$$\begin{cases} \delta \geq 0{,}50 \\ \alpha \geq 0{,}25(0{,}5+\delta)^2\,. \end{cases} \tag{7.74}$$

According to Bathe (1996), $\alpha = 0.25$ and $\delta = 0.5$ are the best choice to avoid response distortion. In fact, Rodriguez (1996) shows that for these values the period elongation is minimized and there is no amplitude decay. By increasing the values of the integration parameters, the total simulation time is substantially decreased. Nevertheless, the response exhibits a larger period elongation and also some amplitude decaying. A general procedure is described below for the nonlinear solution sought around the static equilibrium position.

General procedure

1st Step: At time $t = 0$, build the mass ($\mathbf{M}$), damping ($\mathbf{B}$) and stiffness ($\mathbf{K}$) matrices.

2nd Step: Initialize the displacement ($\mathbf{q}$), velocity ($\dot{\mathbf{q}}$) and acceleration ($\mathbf{q}$) vectors[6].

3rdStep: Given the time step Δt, calculate the auxiliary parameters, Bathe (1996): $a_k(\Delta t, \alpha, \delta)$, $k = 0,1,\ldots,7$.

4th Step: Build the effective stiffness matrix

$$\hat{\mathbf{K}} = \mathbf{K} + a_0\mathbf{M} + a_1\mathbf{B} \tag{7.75}$$

5th Step: For each time step,

Rebuild the damping matrix, $\mathbf{B}$, at instant *t*;

Rebuild the effective stiffness matrix, $\hat{\mathbf{K}}$;

Build the effective load

$${}^{t+\Delta t}\hat{\mathbf{p}} = {}^{t+\Delta t}\mathbf{p} + \mathbf{M}(a_0\ {}^{t}\mathbf{q} + a_2\ {}^{t}\dot{\mathbf{q}} + a_3\ {}^{t}\ddot{\mathbf{q}}) + \mathbf{B}(a_1\ {}^{t}\mathbf{q} + a_4\ {}^{t}\dot{\mathbf{q}} + a_5\ {}^{t}\ddot{\mathbf{q}}). \tag{7.76}$$

Solve the matrix equation

$$\hat{\mathbf{K}}\ {}^{t+\Delta t}\mathbf{q} = {}^{t+\Delta t}\hat{\mathbf{p}}\,; \tag{7.77}$$

Obtain the velocities and accelerations vectors by using eqns (7.72) and (7.73);

Verify the unilateral contact condition;

Determine dynamic tension and curvature.

---

[6] These vectors may be initialized null, for example; the Newmark method should converge to the correct solution.

7.3.9 Illustrative Examples in Frequency and Time Domains

Figures 7.16 and 7.17 present some illustrative examples concerning the same SCR presented in Table 7.1. The simulations considered current and a circular motion imposed on the top. Maximum, minimum and RMS values of dynamic tension and curvature amplitudes are shown along the arch-length of the riser.

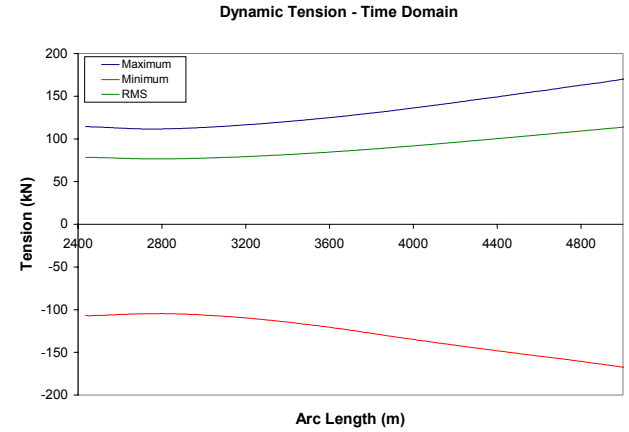

(a)

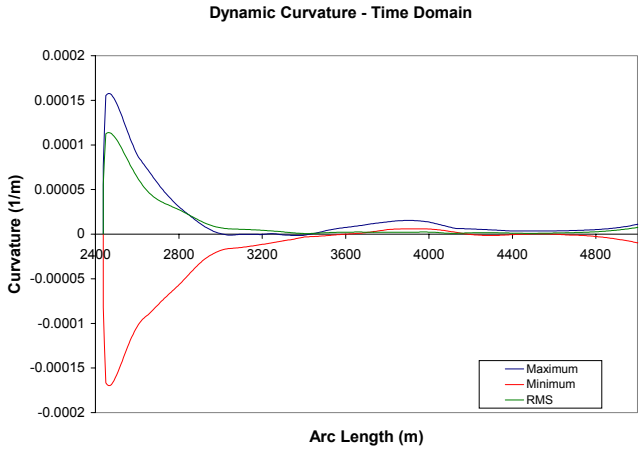

(b)

Figure 7.16: Time-domain dynamic solution for a SCR (Table 7.1). Envelopes of (a) tension; (b) curvature. Motion imposed to the top: A=1.0 m, T=10.0 s. Current profile: current at surface $V_c = 2$ m/s , towards the catenary, with a sheared triangular profile, $v_c(y) = V_c f(y)$; $f(y) = 3y/2H - 1/3$.

Note that the current nonlinear effects cause axial and transversal displacements to be not symmetric far away from the TDP region. Even though it is a minor issue, it can play a role, regarding the possibility of clashing between adjacent risers.

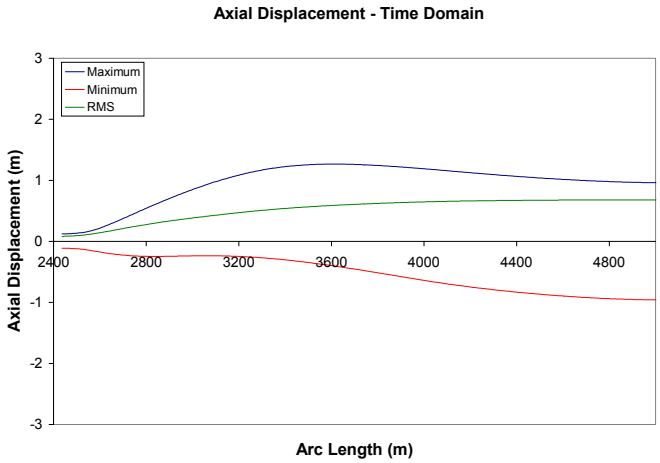

(a)

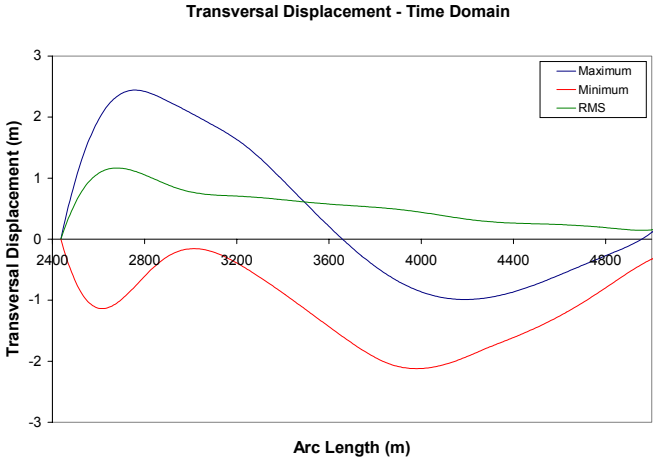

(b)

Figure 7.17: Time-domain dynamic solution for a SCR (Table 7.1). Envelopes of (a) axial displacement; (b) transversal displacement.

Figure 7.18 compares frequency- and time-domain solutions, for a SCR installed in 575 meters depth, from a semi-submersible platform. General data are provided in Table 7.3.

Table 7.3: 16” SCR data.

Parameter	
Axial rigidity EA (kN)	4E+06
Bending stiffness EI (kN m^2)	78000
Immersed weight q (kN/m)	1.19
External diameter D (m)	0.4064
Thickness (mm)	19.05
Depth H (m)	575
Total length (m)	1030
Angle at top θ_L (^{o})	67 (w.r.t. horizontal)
Suspended length L (m)	2571
Tension at TDP T_0 (kN)	694.14
Flexural length λ (m)	10.6
Curvature at TDP χ_0 (m^{-1})	1.077E-03

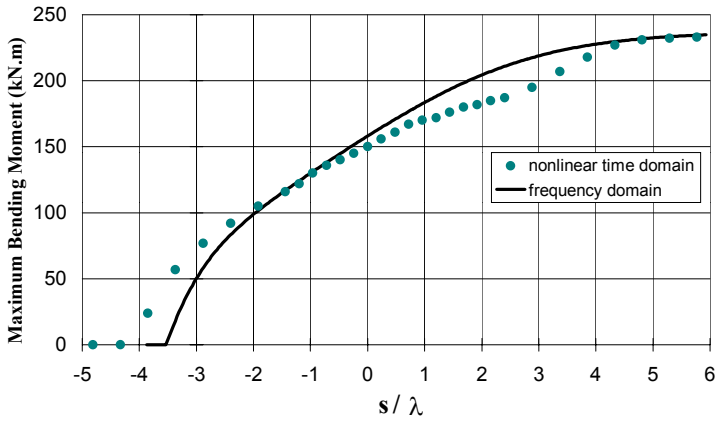

Figure 7.18: Local bending moment at TDP region of a 16’’ SCR in 575 water depth. Comparison between simulations in frequency- and time-domains. No current; severe sea state. Circular motion imposed on the top: ($T_w = 12\,s$; $A = 2.2\,m$).

7.3.10 Dynamic Tension

Dynamic tension in cables has been the subject of thorough analytical studies by a number of authors; see, e.g., the important works by Irvine and Caughey (1974), Triantafyllou (1984), Triantafyllou et al. (1985), Irvine (1992), Leissa and Saad (1994). Recently, Aranha and Pinto (2001), based on Triantafyllou's results and enlarging a previous result, Aranha et al. (1993), derived a closed-form analytical solution for the dynamic tension of a submerged riser, subjected to harmonic motion imposed at the top, under the action of current and waves. Such a study was published with two other companion papers; Aranha et al. (2001a,b), allowing us to treat the important problems of dynamic compression and the analytical estimation of the envelope probability-density function of the dynamic tension in a random sea.

Figure 7.19 presents nonlinear time-domain simulations of dynamic tension for an ideal case where $EI = 0$. Strictly speaking, negative tension should not occur, as shown in Figure 7.20, comparing the analytical prediction to experimental results for the same case. Figures 7.21 and 7.22 present some illustrative results comparing nonlinear time domain results with the analytical solutions.

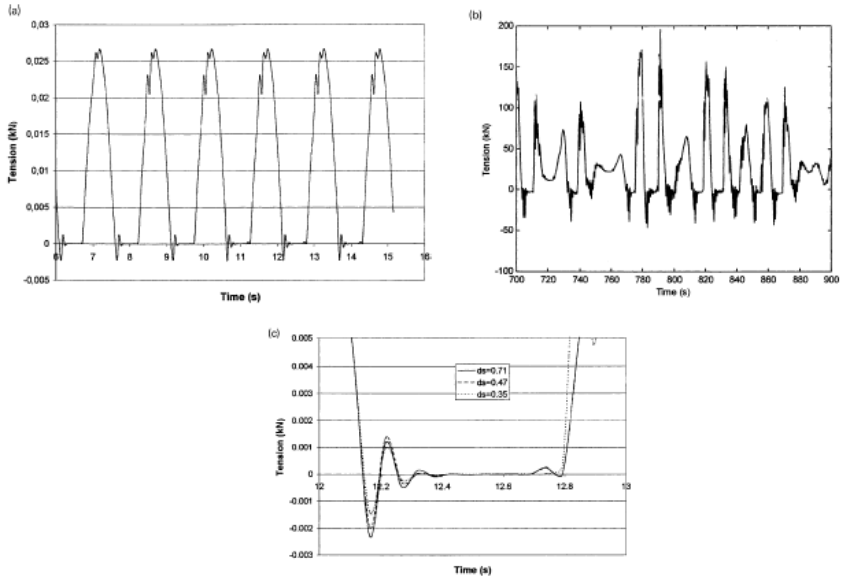

Figure 7.19: Nonlinear time-domain simulations of the dynamic tension at the TDP region of an ideal riser, $EI = 0$, subject to motion imposed on top: (a) harmonic motion; (b) random motion; (c) mesh size dependence; Aranha and Pinto (2001).

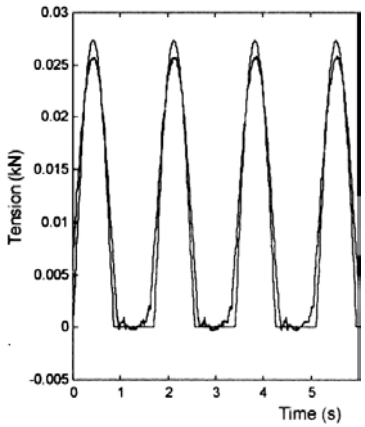

Figure 7.20: Dynamic tension at TDP of an ideal riser, $EI = 0$, subject to harmonic motion imposed on top. Analytical model compared to experimental results. Aranha and Pinto (2001).

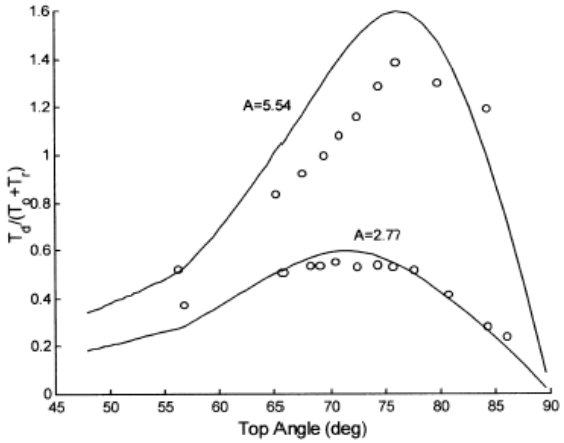

Figure 7.21: Dynamic tension at the TDP of a flexible riser as a function of the angle at top, parameterized in amplitude of motion at top: A=2.77; 5.54 m. Comparison between a nonlinear time-domain code and an analytical solution; Aranha and Pinto (2001). o – time-domain. T_r is a reference limit value for the compression of the flexible riser.

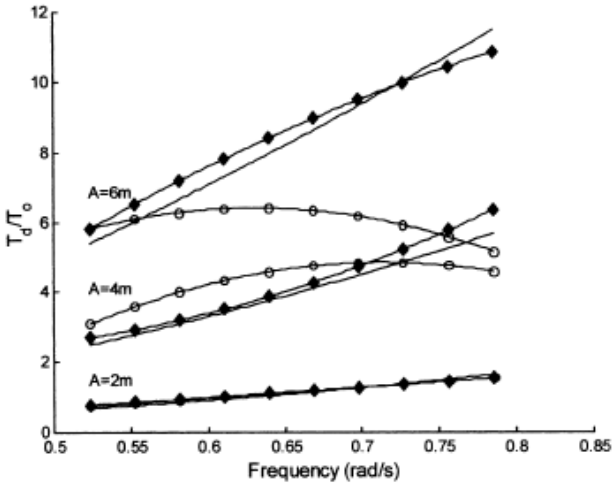

(a)

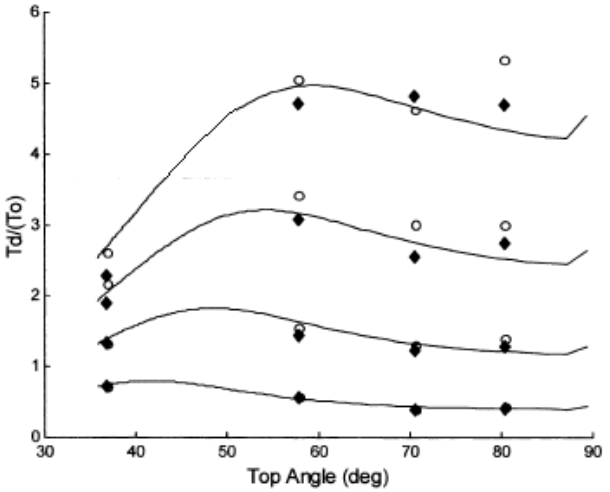

(b)

Figure 7.22: Dynamic tension at the TDP of a SCR, parameterized in amplitude of motion at top, (A=0.9; 1.8; 2.7; 3.6 m), as a function of: (a) frequency and (b) angle at top w.r.t. horizontal. Comparison between two nonlinear time domain codes an analytical solution. o – LM (lumped mass); ♦ FEM; Aranha and Pinto (2001).

7.3.11 Dynamic Compression under Curvature and Twist

One of the major design concerns is to avoid dynamic compression. Typical flexible-pipe structures used to have their engineering properties related to tension and bending loads rather than to compression. Nevertheless, their response to pure compression could trigger loop formation or else the most

catastrophic flexible-pipe failure mode: *bird-caging*. If a steel catenary riser is used instead, dynamic compression may cause high peak values of bending stresses during the post-buckling behavior or even provoke low-cycle (short term) fatigue in severe environmental conditions. Therefore, most of the recent riser-design premises include a new constraint: to establish a geometry avoiding compression. Nevertheless, with the introduction of the FPSO concept and, consequently, more severe motions, the dynamic compression becomes unavoidable to a certain degree. From the designer point of view, not only full nonlinear numerical codes but also analytical approaches are worthwhile, as a critical value for compression is needed as a design criterion.

Aranha et al. (2001a) proposed a stability model, deriving an analytical expression to determine the critical load in risers, subjected to dynamic compression and including the effect of the initial (static) curvature. Their treatment is restricted to the planar problem. The authors point out the importance of an analytic estimate for the critical load based on the difficulty to interpret numerical results around the "saturation region", if a reference value in not known *a priori*. Regarding the effect of the curvature on the critical load, they showed that the analytical expression recovers Euler's critical load in the limit when $\chi \to 0$ (straight beam). On the other hand, for moderately large curvatures, the expression gives a critical load about 9 times higher than Euler's critical load. Several comparisons with numerically obtained results (from full nonlinear simulations, without twisting) were made, indicating a fairly good agreement, in the sense that the numerically determined tensions tend, in fact, to "saturate compression" around the estimated critical load.

By introducing a physical argument, according to which, a 'local buckling length-scale' can be estimated from the classical beam dispersion relation (see, e.g., Whitham, 1974) as,

$$l = \frac{\pi}{k} = \pi \sqrt[4]{\frac{EI}{(m+m_a)\omega^2}}, \tag{7.78}$$

where k is the local flexural wave number, the critical load is shown to satisfy an extended Euler's relation

$$P_{cr} = EI\left(\frac{p\pi}{l}\right)^2, \tag{7.79}$$

where p is the smallest root of the characteristic equation

$$\begin{aligned} &\tan p = p + \frac{p^3}{3} - \frac{p^5}{\gamma^2(_0)} \\ &\gamma(\chi_0) = \frac{1}{8}\frac{l}{\lambda}\overline{\Lambda}(\chi_0)\ ; \quad \overline{\Lambda}(\chi_0) = \frac{1}{2}\chi_0 l\left(\frac{EA}{T_0}\right)^{1/2}. \end{aligned} \tag{7.80}$$

In eqn (7.80), $\overline{\Lambda}$ is the Irvine–Caughey nondimensional parameter (the ratio between axial and geometric rigidities). The critical load is dependent upon the frequency ω of the cyclically imposed tension. It turns out that for small curvature, such that $\chi l \le 10^{-2}$, we obtain $p \cong 1$, recovering Euler's critical value. For moderately large curvatures or upper, such that $\chi l \ge 3\times 10^{-2}$, $p \cong 3$, thus increasing the buckling load value by a factor of 9.

Figure 7.23 shows an example comparing a full nonlinear FEM time-domain simulation with the analytical prediction for the dynamic compressing load.

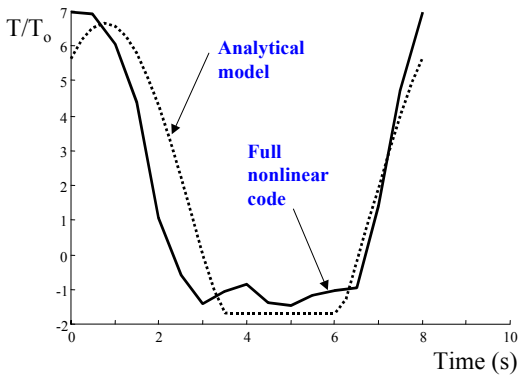

Figure 7.23: A steel catenary riser subjected to harmonic motion at the top and dynamic compression at TDP. Full nonlinear numerical simulation compared to analytical prediction; Aranha et al. (2001a).

$EI = 9241\,\text{kNm}^2$; $(m + m_a) = 108.6\,\text{kg/m}$; $q = 0.307\,\text{kN/m}$;

$T_0 = 134\,\text{kN}$; $P_{cr}/T_0 = 1.65$; T = 8 s; A = 4 m

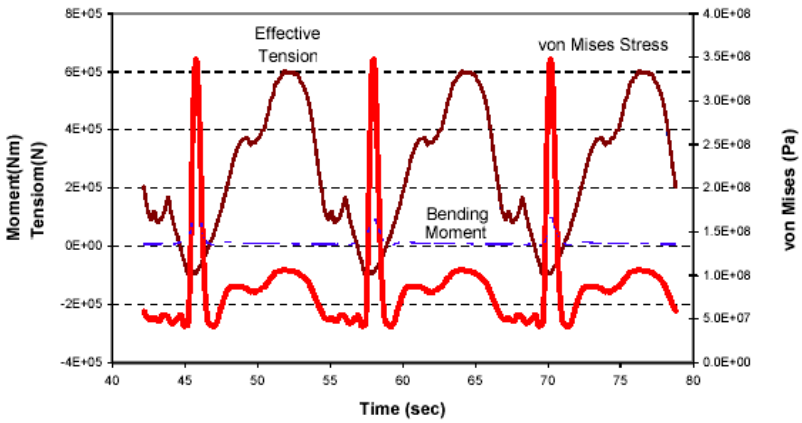

Figure 7.24: Nonlinear time-domain simulation of effective tension, bending moment and Von Mises stress, at the TDP region of a typical SCR; (bending moment peaks coincide with Von Mises stress ones).

Figure 7.24 presents a typical example (an actual design case) of a nonlinear time-domain simulation of tension, bending moment and Von Mises stress at the TDP region of a steel catenary riser. Particularly, the (maximum) Von Mises stress exhibits large and narrowed peak values, corresponding to the rapid increase in bending moment, during the post-buckling stage, when effective tension becomes negative. Note that the riser section is laid on the seabed, being raised periodically as a consequence of dynamic instability caused by

compression. A flexural wave propagates upwards, being extinguished due to the subsequent rise in the cyclic dynamic tension.

Extending Aranha et al. (2001a) reasoning a little further, Ramos and Pesce (2003) considered, from an initial planar configuration, the three-dimensional instability problem, in the Kirchoff sense – see Antman (1974) or Atanackovic (1997). It has been shown that the well-known Greenhill formula can be used to predict stability conditions in risers having an initial curvature and subject to dynamic compression under twisting. The point: 'how to interpret the value of n that appears in Greenhill's expression' has been answered. A *general* procedure was developed, and an analytical tool oriented to the design of risers, specific to stability analysis, was presented.

There are two nondimensional numbers that regulate the instability phenomenon. The first one is the nondimensional curvature $\chi.l$, l being the 'local buckling length scale', determined from the classical beam dispersion relation. The second one is the nondimensional twist, $\tilde{\kappa}_t l$, that gauges the twist under the same length scale. In fact, the nondimensional version of Greenhill relation, can be written as

$$Pl^2/EI + \left((GJ/2EI)\,\tilde{\kappa}_t l\right)^2 = (p\pi)^2, \tag{7.81}$$

where p, being a function of $\chi.l$ and $\tilde{\kappa}_t l$, is the solution of a three-dimensional linear characteristic equation, Ramos and Pesce (2003), asymptotic to eqn (7.80) when twisting is not considered.

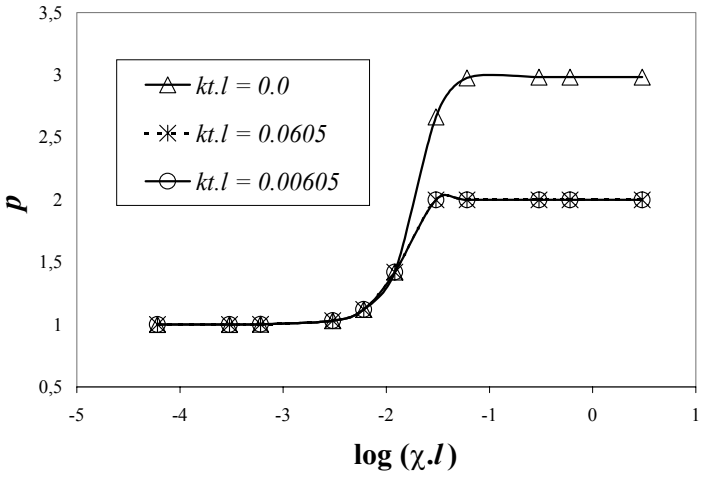

Figure 7.25: Curves of p versus $\log \chi l$ for different values of nondimensional twist $\tilde{\kappa}_t l$. Ramos and Pesce (2003).

From this general theoretical analysis it was inferred that: a) when no twisting is applied to the riser, irrespective of the frequency of oscillation on tension, we have $p \cong n = 1$ for small curvatures ($\chi.l$~0.01), whereas $p \cong n = 3$ for

large curvatures ($\chi.l>0.1$); b), however, if curvature is large enough ($\chi.l>0.1$) and a very small twist is applied, the value of n jumps from 3 to 2, and buckling occurs three-dimensionally, in a quasi-helicoidal form, as could be expected. In regions of moderate curvature, critical load can therefore be overestimated by a factor of 9/4, if twisting is not considered. Twist triggers the instability shape, if two or three-dimensional. Twist is a control parameter of structural instability, in the sense of classical system dynamics terminology. Though intuitive, this latter result has not yet been confirmed experimentally.

7.4 Other Important Issues

This chapter treated the dynamics of risers under an analytical-numerical approach. For the sake of simplicity only the planar problem of catenary risers was addressed, aiming to present an overview on fundamentals and practical issues, regarding design practice. Many other important subjects were not addressed in this chapter.

The important VIV phenomenon was not addressed, deserving an entire and specific treatment. As pointed out before, VIV fundamentals are not yet fully understood; Sarpkaya (2003). Some open issues in VIV, of substantial importance for riser dynamics, may be cited, such as for example, Reynolds-number dependence, multi-modal simultaneous excitation, curvature effects, influence and coupling of VIV with the dynamics in other time-scales, sub-harmonic resonance that couples stream and cross-wise displacements, etc. Regarding sub-harmonic resonance it should be pointed out that, for catenary-risers, eigenfrequencies, corresponding to in-plane and out-of-plane modes, appear interlaced one after the other. For a given reduced velocity range, there would be always the possibility of rational ratios between stream and crosswise frequencies, leading to the appearance of complex multi-branched amplitude response. According to Sarpkaya (2003), page 61, ratios other than 2 lead to “considerably more complex” responses. Moreover, tension oscillation may trigger mode excitation.

Another important issue not treated in the present text refers to the phenomenon of clashing of adjacent risers. Many investigations have been conducted in recent years; see, e.g., Huse (1996), Huse et al. (1998), Huse and Kleiven (2000). Furthermore, studies have been recently reported in which a wake-induced relative motion, with low frequency and large amplitude, is found to be of great importance; Huang and Wu, (2002). These studies point out that the downstream riser may experience loss of dynamic stability, once the current exceeds a critical value, this critical speed being governed by a set of non-dimensional parameters.

Nonlinear effects associated to the action of strakes, end-fittings and intermediate buoys deserve special attention as well. Finally, the crucial riser–soil interaction problem still awaits a comprehensive and consistent treatment, where nonlinear effects would be properly taken into account. Embedding, trenching or shocking should be mentioned as some of important phenomena not yet properly incorporated in most design procedures, deserving much more investigation.

Acknowledgments
The authors acknowledge research grants from CNPq (the Brazilian National Research Council), FAPESP, São Paulo State Research Agency and from the FINEP/CTPETRO program administered by ANP (the National Petroleum Agency). The authors also thank PETROBRAS for the continuous research support on riser engineering. We are especially grateful to Professor José A. P. Aranha, University of São Paulo, for a strong collaborative work, to whom much of the results here presented should be attributed. Finally, we thank Mr. Lauro Massao Yamada da Silveira and Mrs. Rosianita Balena, PhD students, for their help during the preparation of this manuscript. *We dedicate this text to the memory of Professor Octávio Gaspar de Souza Ricardo.*

References

[1] Antman, S.S., Kirchhoff's problem for nonlinearly elastic rods, *Quarterly Journal of Applied Mathematics*, **XXXII**, pp. 221–240, 1974.
[2] American Petroleum Institute, 1998, Recommended Practice 2RD – Design of Risers for Floating Production Systems (FPSs) and Tension-Leg Platforms (TLPs), 1st edn., 163p, 1998.
[3] Aranha, J.A.P., Martins, CA & Pesce, CP, Analytical approximation for the dynamic bending moment at the touchdown point of a catenary riser, *International Journal of Offshore and Polar Engineering*, December **7** (4), pp. 293–300, 1997.
[4] Aranha, J.A.P, Pesce, C.P., Martins, C.A. & Andrade, B.L.R., Mechanics of submerged cables: asymptotic solution and dynamic tension, *Proc. of the 3rd International Offshore and Polar Engineering Conference*, ISOPE'93, Singapore, June 6–11, **II**, pp. 345–356, 1993.
[5] Aranha, J.A.P. & Pinto, M.M.O., Dynamic tension in risers and mooring lines: an algebraic approximation for harmonic excitation, *Applied Ocean Research* **23(2)**, pp. 63–81, 2001.
[6] Aranha, J.A.P.; Pinto, M.O. & Silva, R.M.C., On the dynamic compression of risers: an analytic expression for the critical load, *Applied Ocean Research* **23(2)**, pp. 83–91, 2001a.
[7] Aranha, J.A.P.; Pinto, M.O.& Leite, A.J.P., Dynamic tension of cables in a random sea: analytic approximation for the envelope probability density function, *Applied Ocean Research Research* **23(2)**, pp. 93–101, 2001b.
[8] Atanackovic, T.M., *Stability Theory of Elastic Rods*. World Scientific Publishing Co., Singapore, 1997.
[9] Bathe, K. J., *Finite Element Procedures*. Prentice Hall, New Jersey. 1037 p., 1996.
[10] Bender, C.M & Orszag, S.A., *Advanced Mathematical Methods for Scientists and Engineers*. McGraw-Hill Book Co., International Series in Pure and Applied Mathematics, 593 p., 1978.
[11] Bernitsas, M.M. & Korakakis, J.E., 1988, Importance of nonlinearities in static riser analysis, *Applied Ocean Research*, **10(1)**, pp. 2–9, 1988.
[12] Bowman, F., *Introduction to Bessel Functions*. Dover Publications Inc., 135 p., 1958.
[13] Burridge, R., Kappraff, J. & Morshedi, C., The sitar string: a vibrating-string with a one-sided inelastic constraint, *SIAM Journal of Applied Mathematics*, **42(6)**, pp. 1231–1251, 1982.

[14] Carrier, G.F., Krook, M. & Pearson, C.E., *Functions of a Complex Variable. Theory and Technique*. Hod Books, Ithaca, N.Y., 438 p., 1983.
[15] Chucheepsakul, S. & Huang, T., Effect of axial deformation on natural frequencies of marine risers, *Proc. of the 7th International Offshore and Polar Engineering Conference*, ISOPE'97, Honolulu, May 25-30, **II**, pp. 131–136, 1997.
[16] Huang, S. & Wu, W., Nondimensional parameters governing the onset of wake-induced marine riser collision, *Proc. of the 22nd International Conference on Offshore Mechanics and Arctic Engineering*, OMAE 2003, Cancun, Mexico, June 8-13, paper OMAE2003-37121, 2003.
[17] Huse, E., Experimental investigation of deep sea riser interaction, *Proc. of the OTC 1996*, *Offshore Technology Conference*, Houston, paper No.8070, 1996.
[18] Huse, E., Kleiven,, G., & Nielsen, F.G., 1998, Large scale testing of deep sea risers, *Proc. of the OTC 1998*, *Offshore Technology Conference*, Houston, Paper No.8701, 1998.
[19] Huse, E. & Kleiven, G., Impulse and energy in deep-sea riser collisions owing to wake interference, *Proc. of the OTC 2000, Offshore Technology Conference*, Houston, May, Paper No.11993, 2000.
[20] Irvine, H.M. & Caughey, T.K., The linear theory of the free vibrations of a suspended cable, *Proceedings of the Royal Society London*, **A**. **341**, pp. 299–315, 1974.
[21] Irvine, M., Local bending stress in cables, *Proc. of the 2nd International Offshore and Polar Engineering Conference*, ISOPE 1992, San Francisco, June 1–19, **2**, pp. 342–345, 1992.
[22] Kevorkian, J. & Cole, J.D., 1981, *Perturbation Methods in Applied Mathematics*. Springer–Verlag, Applied Mathematical Sciences, **34**, 558 p,, New York, 1981.
[23] Lambrakos, K.F., Triantafyllou, M.S & Moros, T., Hydrodynamic coefficients for risers with strakes, *Proc. of the 21st International Offshore Mechanics and Arctic Engineering Conference*, OMAE 2002, Oslo, Norway, June 23–28, paper OMAE2002-28221, 2002.
[24] Larsen, C.M., Flexible riser analysis - comparison of results from computer programs. *Marine Structures, Design, Construction and Safety*, **5(5)**, Special Issue on Flexible Risers (Part I), pp. 103–119, 1992.
[25] Leira, B.J. & Remseth, S.N., A comparison of linear and non-linear methods for dynamic analysis of marine risers, *Proc. of the Behavior of Offshore Structures Symposium*, BOSS 1985, Amsterdam, The Netherlands, 1985.
[26] Leissa, A W. & Saad, A M., Large amplitude vibrations of strings, ASME. Transactions, **61**, June 1994, 296–301, 1994.
[27] Love, AE.H., *A Treatise on the Mathematical Theory of Elasticity*. 4th edn., Dover Pub. Inc., N.Y., 643 p., 1944.
[28] Martins, C.A., *An Expeditious Tool for Feasibility Studies of Steel Catenary Risers*, (in portuguese). Thesis of 'Livre Docência', Escola Politécnica, University of São Paulo, 2000.
[29] Martins, C.A., Higashi, E. & Silva, R.M.C., A parametric analysis of steel catenary risers: fatigue behaviour near the top. *Proc. of the 10th International Offshore and Polar Engineering Conference*, ISOPE'2000, Seattle, USA, **II**, pp. 54–59, 2000.

[30] Newberry, B.L. & Perkins, N.C., Analysis of resonant tangential response in submerged cables resulting from 1-to-1 internal resonance, *Proc. of the 7th International Offshore and Polar Engineering Conference*, ISOPE'97, Honolulu, May 25-30, **II**, pp. 157–163, 1997.

[31] Patel, M.H. & Seyed, F.B., Review of flexible riser modelling and analysis techniques, *Engineering Structures*, **17(4)**, pp. 293–304, 1995.

[32] Pesce, C.P., *Mechanics of Submerged Pipes and Cables in Catenary Configuration*, (in portuguese), Thesis of 'Livre Docência', Escola Politécnica , University of São Paulo, 350 p., 1997.

[33] Pesce, C.P., Aranha, J.A.P., Martins, C.A., Ricardo, O.G.S. & Silva, S., Dynamic curvature in catenary risers at the touch down point: an experimental study and the analytical boundary layer solution. *International Journal of Offshore and Polar Engineering*, **8(4)**, pp. 302–310, 1998a.

[34] Pesce, C.P., Aranha, J.A.P., Martins, C.A., The soil rigidity effect in the touch down boundary layer of a catenary riser: static problem. *Proc. of the 8th International Offshore and Polar Engineering Conference*, ISOPE'98, Montreal, May 24-29, **II**, pp. 207–213, 1998b.

[35] Pesce, C.P., Fujarra, A.L.C., Simos, A.N. & Tannuri, E.A., Analytical and closed form solutions for deep water riser-like eigenvalue problem. *Proc. of the 9th Int. Offshore and Polar Engineering Conference*, ISOPE'99, Brest, France, June 1-6, **II**, pp. 255–263, 1999.

[36] Pesce, C.P. & Martins, C.A. Riser-soil interaction: local dynamics at TDP and a discussion on the eigenvalue problem, *Proc. of the 23rd International Conference on Offshore Mechanics and Arctic Engineering*, Vancouver, Canada, June 20–25, paper OMAE2004-51268, 2004.

[37] Ramos Jr, R.; Pesce, C. P., A stability analysis of risers subjected to dynamic compression coupled with twisting, *Journal of Offshore Mechanics and Arctic Engineering*, **125**, pp. 183–189, 2003.

[38] Rodriguez, G. P. S., *On the Direct Integration of a Linear System of First and Second-order Differential Equations*. PhD Thesis (in portuguese). University of São Paulo, 160p., 1996.

[39] Sarpkaya, T., On the force decompositions of Lighthill and Morison, *Journal of Fluids and Structures*, **15(2)**, Feb. 2001, pp. 227–233, 2001.

[40] Sarpkaya, T., *Critical Review of the Intrinsic Nature of Vortex Induced Vibrations*. Naval Postgraduate School, Monterey, California, Report no. NPS-ME-03-002. 126 p., 2003.

[41] Silveira, L.M. & Martins, C.A. Nonlinear time-domain analysis of risers. *Proc. of the 17th International Congress of Mechanical Engineering*, COBEM2003, November 10-14, S. Paulo, Brazil, paper 1398, 2003.

[42] Triantafyllou, M.S., The dynamics of taut inclined cables. *Quarterly Journal of Mechanics and Applied Mathematics*, **37**, pt. 3, 1984.

[43] Triantafyllou, M.S., Bliek, A. & Shin, H., Dynamic analysis as a tool for open sea mooring system design, *Proc. of the Annual Meeting of The Society of Naval Architects and Marine Engineers*, November 1985, N.Y., 1985

[44] Vikestad, K., Vandiver, J.K. & Larsen, C.M., Added mass and oscillation frequency for a circular cylinder subjected to vortex-induced vibrations and external disturbance. *Journal of Fluids and Structures*, **14**, pp. 1071–1088, 2000.

[45] Whitham, G.B., *Linear and Non-linear Waves*, Pure and Applied Mathematics, Wiley-Interscience Series of Texts, Monographs and Tracts, 636 pp., 1974.

Chapter 7 - Index

Chapter 7 - Table of Contents